Uniaxial and Biaxial Restraint in Concrete Pavement Undergoing Alkali-Silica Reaction

by

Romit Thapa

Submitted in Partial Fulfillment of the Requirements

for the Degree of

Master of Science in Engineering

in the

Civil and Environmental Engineering Program

YOUNGSTOWN STATE UNIVERSITY

August 2018

Uniaxial and Biaxial Restraint in Concrete Pavements with Alkali-Silica Reaction

Romit Thapa

I hereby release this thesis to the public. I understand that this thesis will be made available from the OhioLINK ETD Center and the Maag Library Circulation Desk for public access. I also authorize the University or other individuals to make copies of this thesis as needed for scholarly research.
Signature:

_____

Romit Thapa, Student Date

Approvals:

_____

Dr. Richard A. Deschenes, Thesis Advisor Date

_____

Dr. AKM. Anwarul Islam P.E., Committee Member Date

_____

Dr. Jai K. Jung, Committee Member Date

_____

Dr. Salvatore A. Sanders, Dean of Graduate Studies Date

ABSTRACT

Alkali-silica reaction (ASR) is a durability issue in concrete structures that leads to expansion, cracking, and deterioration in concrete properties. Temperature, humidity, alkali level, reactivity of aggregate and confinement stresses are the major factors effecting the development of ASR. The primary objective of this study was to investigate the influence of compressive stress on the development of ASR-induced expansion, cracking and degradation of mechanical properties of concrete pavement.

The research project was conducted at Youngstown State University in which nine 10 in. concrete cubes were fabricated and monitored for ASR expansion. The mixture design used a typical Federal Highway Administration (FHWA) cement content of 564 lb/yd^3 to better represent the mechanical properties of concrete pavement. The water cement ratio was 0.47. The reactive fine aggregate and coarse aggregate were used in the natural gradation. The concrete cubes were subjected to different level of confinement stresses namely, uniaxial with 435 psi (3 MPa) in X direction and biaxial with 363 psi (2.5 MPa) and 435 psi (3 MPa) in Y and Z direction respectively. The cube specimens were stored at temperature of 38ºC and 100% RH. Strain measurements were taken periodically with detachable mechanical (DEMEC) gauge and studs embedded into the concrete, and modulus of elasticity and compressive strength of samples were determined. After the exposure period, samples were prepared and inspected following the damage rating index (DRI) procedure. Finally, the damage mapping of three different plane of each samples were created.

Strain measurements showed that the strain in the unrestraint direction was greater than that in the restraint direction. Similarly, strain was reduced in the direction of stress applied

in both stress states and transferred to the unrestraint direction. DRI test showed that the ASR-induced damage varies with different stress states. Moreover, DRI values for unrestraint cube specimens were considerably higher than the biaxial and uniaxial stress state concrete specimens. The confinement stresses were unable to suppress reaction but were successful to reduce the degree of damage.

ACKNOWLEDGEMENTS

First and foremost, I have to thank my grandmother Shubadhra Thapa, my father Bidur Kumar Thapa and mother Susan Thapa for their love, inspiration and support throughout my life. I sincerely appreciate the unfailing love and continuous motivation of my wife Sahara throughout my years of study and through the process of researching and writing this thesis. My elder sisters Ruby and Rosy deserve my wholehearted thanks as well.

I would like to thank my thesis advisor Dr. Richard Deschenes of the Civil & Environmental and Chemical Engineering at Youngstown State University. The door to Dr. Deschenes office was always open whenever I ran into a trouble spot or had a question about my research or writing. His support and review of the work throughout the research were invaluable. I am thankful to Dr. Deschenes for his great help and guidance in casting, loading and testing of specimens. I am also deeply grateful to the committee member, Dr. AKM. Anwarul Islam, for his wonderful guidance and suggestions to accomplish this research. I am highly indebted to my thesis committee member, Dr. Jai K. Jung for his willingness to serve on my thesis committee and providing me with valuable suggestions and feedbacks.

I would like to acknowledge the academic and technical support of the YSU and its staff, particularly to Ms. Linda Adovasio for her support and assistance. I am indebted to the technicians at the machine shop, who provided me the mechanical tools, assisted me to cut the plywood, rods, and in making detachable mechanical studs.

Finally, to all my friends, thank you for your understanding and encouragement in many moments of crisis. Your friendship makes my life a wonderful experience.

TABLE OF CONTENTS

LIST OF FIGURES

LIST OF TABLES

LIST OF ABBREVIATIONS

AASTHO	American Association of State highway and Transportation
AMBT	Accelerated Mortar Bar Test
ASR	Alkali-Silica Reaction
ASTM	American Society for Testing Materials
CPT	Concrete Prism Test
DEMEC	Detachable Mechanical
DRI	Damage Rating Index
FHWA	Federal Highway Administration
JPCP	Jointed Plain Concrete Pavement
ISE	Institute of Structural Engineers
ITZ	Interstitial Transition Zone
RH	Relative Humidity
YSU	Youngstown State University

Chapter 1 Introduction

1.1. Background

Concrete is a widely used and durable material throughout the world. It is used in almost every type of structure that we build today including dams, highways, buildings, bridges, and pavements. Usually, concrete structures are designed to last from 50 to 100 years (Funahashi, 1990). Unfortunately, concrete structures are subjected to environmental conditions that can cause deterioration in concrete, leading to structural failure. Among them, the alkali-silica reaction (ASR) is one of the many factors that might be responsible for the deterioration and premature loss of serviceability of concrete infrastructures. The alkaline pore solution in cement may react with certain unstable siliceous phases, present in certain aggregate (such as chert, opal, quartz, dolomite and volcanic glass). The reaction precipitates as a gel, which then swells as it draws water from the cement paste. As a result, the gel exerts pressure on the aggregate particles and cement causing cracks in the concrete structure. This ASR mechanism is deleterious when swelling strength of gel exceeds the tensile strength of concrete and causes cracks in concrete (Moranville-Regourd, 1997).

Since the initial discovery of ASR in the late 1930s, there have been numerous reported cases of ASR in concrete structures particularly highway structures and pavements in a number of states in the USA and throughout the world (Stanton, 1940). For instance, a recent 12-miles sections of jointed plain concrete pavement (JPCP) on Interstate 530 near Pine Bluff, AR. and a 16-miles section of concrete pavement along US 113 in Georgetown, DE were identified with the symptoms of ASR as reported by the U.S. Department of Transportation under Federal Highway Administration (FHWA) (M. D. Thomas et al., 2013). Similarly, ASR-induced damages were observed in airfield pavements on at least

nineteen U.S. air bases, six Navy , three Army airfields and at least eight commercial U.S. airports (Giebson et al., 2010).

Ensuring the safety of ASR-affected concrete structure has always been a challenging task. It is important to understand the progression of cracking and deterioration of mechanical properties to evaluate the performance of ASR-affected concrete structures (Swamy and Al-Asali, 1988; Ahmed et al., 2003; Giaccio et al., 2008). The damage rating index (DRI) is a method of evaluating the performance of ASR-affected concrete structures. This method is most widely used to monitor micro-cracks in ASR-affected concrete structures. The DRI method can be applied without a reference measurement (Sanchez et al., 2015). It has been extensively applied to the cores of existing structures as well as to laboratory concrete specimens. In a similar manner, the degradation of mechanical properties such as compressive and tensile strength and elastic modulus of the ASR affected concrete has been evaluated by various authors under unconstrained conditions (Ahmed et al., 2003; Lindgård et al., 2013; Sargolzahi et al., 2010). However, these properties can be influenced by stress-state and it is important to understand the influence of anisotropic restraint on the properties of ASR-affected concrete structures and pavements. The objective of this research is to evaluate the influence of anisotropic stress states on the development of ASR in concrete pavement and the results of Gautam (2016) were compared to the results of this thesis.

1.2. Research Scope

The influence of anisotropic stress states on concrete pavement were evaluated through a combination of strain measurements, mechanical properties tests, and petrographic methods. A total of nine concrete cube specimens were made with dimensions of 10 x 10

x 10 in. (254 x 254 x 254 mm) Specimens with uniaxial with 435psi (3MPa) pressure, biaxial with 435 psi (3MPa) and 363 psi (2.5 MPa) pressure, and no restraint were exposed to conditions that accelerate the development of ASR deterioration. Strain was measured periodically, and mechanical properties were tested. After the exposure period, samples were prepared and inspected following the DRI procedure and DRI mapping of samples were done for visualization of the data. The influence of deterioration was assessed for each stress-state and the results were analyzed to gain an understanding of how an anisotropic stress states influence the properties of concrete pavement.

1.3. Thesis Organization

Chapter 2 includes a discussion on the background including definition, history, and factors affecting ASR in concrete structures in order to better define specific aspects of ASR-affected concrete pavements addressed in this thesis. The second part of this chapter includes a literature review of ASR. The mechanisms, symptoms, degradation of mechanical properties due to ASR, factors affecting ASR expansion and prevention method of ASR are highlighted in this chapter. Chapter 3 is a summary of various methods and materials used throughout the research. The chapter provides a step by step description of formwork preparation, casting of concrete cube specimens, type of material used, and different test methods used to measure ASR expansion. Chapter 4 is a summary of the result and discussion. The analyses of data collected throughout the research are presented and described in this chapter. Finally, the research findings, conclusion and recommendation for future improvement are summarized in Chapter 5. Design calculations for high-strength bolts and base plates, and strain measurements are included in the Appendices.

Chapter 2 Literature Review

2.1. Alkali-Silica Reaction

Alkali-silica reaction is a reaction between alkali hydroxides in the pore solution and certain phases of silica present in some aggregate. The reaction produces an alkali-silica gel with varying amounts of calcium that swells as it absorbs moisture. This generates tensile stresses in the concrete that may eventually result in axial and volumetric expansion of the concrete, which may lead to cracking (Stanton, 1940; Swamy, 2002). By the definition of ASR, it is known that there are three important conditions necessary for ASR to occur (Figure 2-1), which are:

(i) A sufficient reactive siliceous mineral phase present in aggregate,

(ii) A sufficient source of alkali from Portland cement or aggregates,

(iii) A sufficient source of moisture.

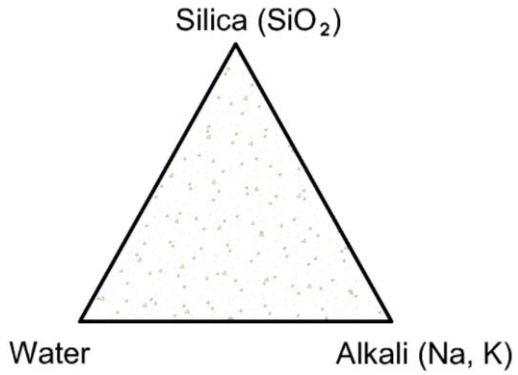

Figure 2-1 Requirements for ASR (M. D. A. Thomas et al., 2011).

2.2. Mechanisms of Alkali-Silica Reaction

The alkali-silica reaction is a slow process and typically takes between 5 and 12 years for visible deterioration to develop. However, the reaction can be more severe in when alkali concentration in pore solution is higher. In a guideline published by Institute of Structural Engineers (ISE), it was reported that ASR development requires sufficient quantities of

reactive silica, water-soluble alkalis, and moisture (ISE, 1992). If any of these condition are not met, the reaction will not occur. The ASR mechanism is illustrated in the Figure 2-2 where step by step progression of the reaction is shown. First, the ASR gel is produced as a result of reaction between alkali and silica which is present inside the concrete then it absorbs water which leads to swelling of gel eventually causing cracks in concrete. The reaction can be divided into two different stages (Swamy, 2002). The first stage being the hydrolysis of reactive silica by OH^- to form an alkali-silica gel. The alkali (R^+ denotes an alkali ion such as Na^+ and K^+) are introduced into concrete, mostly by Portland cement, which is weakly bonded to hydroxyl ions. The weak bond allows compounds to dissolve into solution becoming free ions. The acidic reactive silica found in aggregate is unstable and will dissolve in the basic solution (NaOH, KOH) with a high pH value of 13.5 to 13.9 producing an alkali-metal-ion hydrous silicate gel (N-S-H, K-S-H) in aggregate cracks and cement paste.

$$SiO_2 + R^+OH \rightarrow R^+SiO_{(aq)}\,(\text{Alkali-silica gel}) + SiOH$$

$$SiOH + R^+OH \rightarrow R^+SiO_{(aq)}\,(\text{Alkali-silica gel}) + H_2O$$

In the second stage, the hygroscopic gel absorbs water from the pore solution and expands into available space.

$$R^+SiO_{(aq)} + nH_2O \rightarrow R^+SiO(H_2O)_n\ (\text{Expansive alkali-silica gel})$$

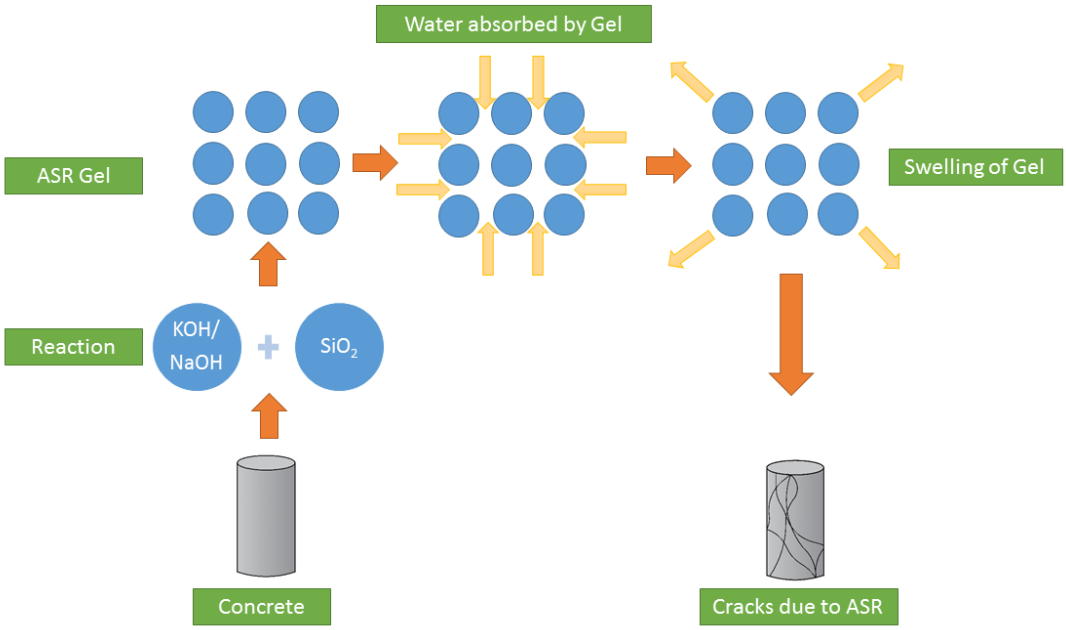

Figure 2-2 Mechanism of Alkali-silica reaction

However, humidity, temperature, aggregate size, paste porosity, and supplementary cementitious material can also affect the rate of ASR reactivity. Some studies have concluded that a minimum internal relative humidity of 80% is required for ASR expansion and that the maximum expansion occurs when the relative humidity is between 95% and 100% (Fournier, 2010; Stark, 1991). Likewise, increases in temperature increases the rate of ASR reaction. The type of reactive siliceous minerals present in the aggregate and size of aggregate considerably impact the rate of alkali-silica reaction. Numerous experiments have been performed on different type of aggregates and effect of particle size of reactive siliceous aggregate on the expansion due to ASR (Dunbar and Grattan-Bellew; Shrimer et al.; Grattan-Bellew and Mitchell; Sanchez, Fournier, Jolin, and Duchesne). It was also found that when two differently sized aggregates were used, ASR expansion decrease with the proportion of small particles (Stéphane Multon et al., 2010). Likewise, use of certain supplementary cementitious materials such as fly ash, meta-kaolin, slag cement, and silica fumes are regarded as the most effective techniques to prevent or minimize the ASR-

induced expansion (Justice et al., 2005; Latifee, 2016). Hence, the rate of ASR can be affected by many factors, resulting in differing responses between mixes and specimens.

2.3. ASR-induced Concrete Degradation

Generally, ASR research is focused on investigating ASR induced expansion, cracking, and degradation of mechanical properties in concrete specimens. Expansion and cracking of the concrete structures are the direct result of swelling of reaction products whereas the third property is the outcome of cracks formation within aggregate, concrete, and the interstitial transition zone (ITZ).

2.3.1. Expansion

Expansion in concrete undergoing ASR is due to the formation of an osmotic pressure gradient between the alkali-silica gel and pore solution (Swamy, 2002) . In recent years, extensive research has been conducted at the aggregate and concrete level using unrestrained specimens to understand the fundamental aspects of the reaction and its occurrence. However, concrete structures are effected by restraint of reinforcement in one or multiple directions (Gautam, 2016). Therefore, in ASR affected concrete structures, stress is generated in steel reinforcement as well as in the concrete (Fujii et al., 1986). This makes the expansion due to ASR more complex. Hence, the expansion measured in the unrestrained specimens cannot appropriately justify the expansion in the actual concrete structure and it is important to explain the relationship between the unrestrained expansion and the ASR-induced expansion with various degree of restraint.

Numerous papers have been published in which concrete specimen undergoing destructive ASR have been submitted to uniaxial restraint stress. In such studies, compressive stress has been applied so as to suppress the expansion (Multon and Toutlemonde, 2006; Berra

et al., 2010; Kagimoto et al., 2014; Takahashi et al., 2015, Gautam, 2016). An important conclusion reached by these researchers is that expansion is decreased by the applied stress and transferred to unrestrained direction. Therefore, the relationship between ASR-induced expansion and the multi stress state becomes more complex due to the process of reduction and transfer of expansion. Different authors have found that the pressure exerted by the ASR gel to be in range between 3MPa to 10 MPa (Le Roux et al., 1992; Sellier et al., 1995; Prezzi et al., 1997). However, the relationship between ASR expansion and multiaxial stress condition was inadequately understood. Previous laboratory studies have provided some information on the effect of biaxial and triaxial restraint stress on ASR-induced expansions (M. D. A. Thomas et al., 2011; Rivard et al., 2002). Multon and Toutlemond (2006) measured the expansion of concrete cylinder (5.1 x 9.5 in.) subjected to multiaxial stress. In this case the author concluded that "the ASR volumetric imposed strain can be considered as constant whatever the stress state" (Gautam, 2016). In contrary, Bishnu et al (2015) and Gautam at al. (2010) found that strain varies with the stress state in a study done using a concrete cube (10 x 10 in.) specimen submitted to multiple stress states. However, both of these studies revealed that expansion was transferred from the restrained to unrestrained direction. However, the knowledge of a possible correlation between expansion and multi-stress state in ASR-effected concrete is inadequate.

2.3.2. Cracking

Cracking is one of the symptoms of ASR concrete. A network of surface cracks or "map cracking", can be observed on many ASR-affected concrete structures. The swelling of the reaction product can generate excessive tensile stress in concrete. As a result, this cause microcracks within the aggregate particles, cement paste and then surface cracking of

concrete structure. Several studies have demonstrated that the traditional approaches including the measurement of the compressive strength of the affected concrete sheds limited light on the ASR-affected concrete. It is found that, as the reaction progresses, the modulus of elasticity decreases while the compressive strength may not change or be reduced (Swamy and Al-Asali, 1988). Quantitative assessment of cracks (such as The DRI) within the affected concrete can be an effective method of assessing damage in existing concrete structures (Rivard and Saint-Pierre, 2009).

Petrographic methods such as the DRI are essential tools for diagnosis and prognosis of ASR in the damaged concrete structures(Dunbar and Grattan-Bellew, 1995; Shrimer et al., 2000 ; Grattan-Bellew and Mitchell, 2006; Sanchez, Fournier, Jolin, and Duchesne, 2015; Sanchez, Fournier, Jolin, Bedoya, et al., 2016). The DRI is a semi-quantitative method performed with the use of a stereomicroscope. First, a concrete specimen is cut and polished to produce a surface for inspection. A 1 cm^2 grid is then traced onto the surface to locate petrographic feature of interest. The occurrence of various petrographic features is then counted for each cell within the grid. The number of occurrences of each feature of interest is then multiplied by a weighting factor and summed to determine the DRI number of the specimen. Finally, the total is then normalized to a surface area of 100 cm^2 for comparison to other specimens. The number of counts corresponding to each petrographic feature of ASR is then multiplied by the weighing factor. In order to reduce the variability between the multiple operators performing the DRI test, the weighing factors have been modified (Villeneuve et al., 2012). A study conducted by Sanchez (2010) using the modified DRI method revealed that the DRI values increased linearly with increasing expansion and that no differences in DRI numbers were observed between the concretes

made with fine or coarse reactive aggregates (Sanchez, 2010). While the DRI method has been applied to laboratory specimens as well as to cores of existing concrete structures, the effect of stress state on damage has not been adequately understood.

2.3.3. Degradation of Mechanical Properties

The degradation of mechanical properties due to ASR-induced expansion has been studied by several researchers. The relationship between expansion and degradation of mechanical properties are vital to the assessment of ASR-affected concrete structures. Most of the reports indicate that there is significant loss of mechanical properties due to ASR (Swamy and Al-Asali, 1988; Morenon et al., 2017; Giaccio et al., 2008). Generally, ASR generates a rapid reduction of tensile strength and modulus of elasticity. Moreover, the compressive strength was less affected and began to drop only at higher level of expansion (Smaoui et al., 2005). Swamy and Al-Asali (1988) studied the flexural strength, modulus of elasticity and compressive strength of the concrete affected by ASR. According to the authors, for expansion up to 0.1%, loss in flexural strength was 50 percent, whereas loss in modulus of elasticity amounted to 20%. However, there was no significant loss in compressive strength at expansion up to 0.1%. On the other hand, H. Marzouk and S. Langdon (2003) reported that results of recent studies showing the compressive strength of normal strength concrete containing a highly reactive aggregates decreased by 28% while the modulus elasticity decreased by 80%. Similarly, it was found that the tensile strength was very sensitive to the effect of ASR and decreased by 30% (Marzouk and Langdon, 2003).

2.4. Test Methods

In this experiment, several mechanical-property and ASR test methods were conducted to assess the materials and reactivity of the concrete used. The tests included compressive

strength, elastic modulus, concrete prism test, accelerated mortar bar test, and the damage rating index. The accelerated mortar bar and concrete prism test were carried out following ASTM C1260 and ASTM C1293, respectively. Compressive strength was tested in accordance with ASTM C39, while the elastic modulus was measured in accordance with ASTM C469. Finally, assessment of internal damage in concrete cube specimens were carried following the DRI method.

2.4.1. ASTM C1260: Accelerated Mortar Bar Test (AMBT)

The ASTM C1260, originally proposed by Oberholster and Davis in 1986, is a 16 day accelerated test to determine the potential deleterious alkali-silica reactivity of aggregates. In this method, the mortar bars are exposed to a 1N NaOH solution at an elevated temperature of 80 °C (ASTM C1260, 2001). This process is useful for aggregates that reacts slowly but can be too harsh for certain aggregates. It does not provide the reactivity of specific cement-aggregate combination, but rather the potential reactivity of the aggregate being evaluated. The mix design and grading are summarized in the Table 2.1 and Table 2.2. The mortar bar dimensions are 1 x 1 x 11.25 in. (25 x 25 x 285 mm) (ASTM C1260, 2001). The bars remains in the mold for 24 ± 2h after casting (Figure B-1 (a)). The bars are then stored in water at 80 °C for 24 ± 2h before the initial length-change is recorded. After the initial reading, the mortar bars are moved into a 1N NaOH solution as shown in the Figure B-1 (b). At least three intermediate readings over a 14 day period should be taken, at approximately the same time each day. Mortar that expands between 0.10% and 0.20% after 14 days are potentially deleteriously reactive. Whereas, expansions less than 0.1% indicate the aggregate to be innocuous. Expansion more than 0.2% indicate the aggregate as deleteriously reactive (ASTM C1260, 2001).

The major limitation of this test is that aggregate without any history of ASR can sometimes test positive due to be its harsh test environment. Therefore, aggregates which test positive should be evaluated using the concrete prim test (CPT) method.

Table 2-1 Mix design for AMBT as specified by ASTM C1260.

Material	Cement	Aggregate	W/C
Weight (g)	440	990	0.47

Table 2-2 Grading requirements as specified by ASTM C1260.

Sieve Size		Mass,%
Passing	Retained on	
No. 4	No.8	10
No.8	No. 16	25
No. 16	No. 30	25
No. 30	No. 50	25
No. 50	No. 100	15

2.4.2. ASTM C1293: Concrete Prism Test (CPT)

The CPT method is used to determine the reactivity of siliceous coarse or fine aggregate in concrete. The AMBT has several limitation and results from certain aggregates may not be reliable. In addition, it is only applicable to evaluate aggregates in mortar sample and this does not correlate to expansion in the field. The CPT was introduced to more precisely identify the potential for deleterious ASR expansion of concrete. It is regarded as the most reliable test procedure, but requires at least 1 years for results. In this test, concrete prisms should be made from cement that meets the requirements for a Type I Portland cement as specified in C150 and have a total alkali content of 0.9 ± 0.1% Na_2O equivalent. The alkali content of the concrete is further increased to 1.25% Na_2O equivalent by adding NaOH into the mixing water. The mix design and grading requirements are summarized in Table 2-3 and Table 2-4 respectively. The water-cement ratio should be maintained in the range

of 0.42 to 0.45 (ASTM C1293, 2008). At least three concrete prims are cast with standard dimension of 3 x 3 x 11.25 in. (75 x 75 x 285 mm) All the prims must then be stored in sealed container that produce a stable environment at 38°C ± 2 °C and 100% RH environment (ASTM C1293, 2008). The prims should be demolded at the age of 23.5 ± 0.5 h and initial length reading should be made. Subsequent readings should be taken of 7, 28, 56 days, 3, 6, 9, and 12 months. If required, addition reading can be taken at 6-month intervals out to 2 years (ASTM C1293, 2008). Before taking readings, the container must be removed from the storage area and stored at 21 °C for 16 ± 4h before reading. The storage container and length-change apparatus are shown in the Figure C-1.

Table 2-3 Mix design for CPT as specified by ASTM C1293

Material	Cement	Rock	Sand	Water
Weight (lb/yd^3)	708	1789	1206	319

Table 2-4 Grading requirements as specified by ASTM C1293

Sieve Size		Mass,%
Passing	Retained on	
3/4in.	1/2in.	33
1/2in.	3/8in.	33
3/8in.	No. 4	33

2.4.3. ASTM C39: Compressive Strength of Cylindrical Concrete Specimens

The compressive strength of concrete is typically a useful indicator of the concrete mechanical properties. Compressive axial load is applied to a cylinder until failure occurs. The load application rate should be within the prescribed range. The compressive strength is calculated by dividing the maximum load reached by the cross-sectional area of cylindrical concrete specimens (ASTM C39, 2001).

The testing machine should be capable of providing sufficient load continuously and without shock. The machine should have enough space to accommodate test specimens in a readable position. The testing machine should be calibrated on an annual basis. It should be equipped with two steel bearing blocks, one of which seats on the upper surface of a specimen, and the other block on which the specimen will be placed on. It is important to go through entire specification before carrying out ASTM C39 (ASTM C39, 2001).

2.4.4. ASTM C469: Standard Test Method for Modulus of Elasticity

This test method is used to determine the stress to strain value and a ratio of lateral to longitudinal strain for a concrete mixtures. It is important to determine the compressive strength of the concrete cylinder prior to performing the ASTM C69 test (ASTM C39, 2001) . One compressometer is attached to cylindrical concrete specimen, parallel to the axis and centered about mid-height of the specimen. After attaching the compressometer, the specimen should be tested at least two time, to 40% of the cylinders compressive strength to properly seat the gages (ASTM C469, 2014). The load should be applied continuously without any shock. The test speed of the machine of screw type should be 0.05 in/min and in hydraulically operated machines should be 35±7 psi/sec (0.24±0.05 MPa/sec). The applied load and longitudinal strain should be recorded without interruption of loading. The longitudinal strain is the total longitudinal deformation divided by the effective gage length. If Poisson's ratio is to be determined, transverse strain should be recorded at the same point without interruption of loading. For this research, we did not conduct the Poisson's ratio test. The calculation of modulus of elasticity should be to the nearest 50,000 psi whereas Possion's ratio should be to the nearest 0.01 (ASTM C469, 2014).

2.4.5. Damage Rating Index (DRI)

The Damage Rating Index (DRI) method, developed in the 1990s, is a tool for assessing the internal damage due to ASR and other durability issues (Grattan-Bellew and Danay, 1992). It is a useful technique to diagnose the cause of concrete deterioration and the extent and progression of deterioration. Recent studied by several authors have improved on and modified the original DRI method (Sanchez, Fournier, Jolin, and Duchesne, 2015; Sanchez, Fournier, Jolin, Bedoya, et al., 2016) . The presence of micro-cracking in aggregates and/or cement paste, reaction product, reaction rims and loss of cement paste-aggregate bond can be observed in the petrographic test of ASR affected concrete.

The test method involves first cutting the concrete core of specimen to provide flat surface for inspection. Then, the surface was progressively polished using hand-polisher with diamond-impregnated rubber disks to provide a surface with defects smaller than approximately 5µm. The polished slices are then sub-divided into a 1 cm by 1 cm cells. Each cell is then observed under a stereomicroscope (15x magnification) and the petrographic features are counted. The petrographic features are then multiplied by the respective weight factor and finally summed. These features and respective weight factors, which were used in this study, were proposed by Villeneuve et al. (2012) and are summarized in Table 3-4. Finally, the sum is normalized to 100 cm^2 (16 in^2) to present the DRI value for each plane.

Table 2-5 Features and weight factors in an individual grid as per the DRI method (Villeneuve et al. 2012).

Petrographic features Weighting factors	**Weight**
Closed/tight cracks in coarse aggregate particle (CCA)	0.25
Opened cracks or network cracks in coarse aggregate particle (OCCA)	2
Cracks or network cracks with reaction product in coarse aggregate particle (OCAG)	2
Debonded coarse aggregate (CAD)	3
Disaggregated / corroded aggregate particle (DAP)	2
Cracks in cement paste (CCP)	3
Cracks with reaction product in cement paste (CCPG)	3

Chapter 3 Materials and Methods

3.1. Introduction

A very highly reactive fine aggregate (per ASTMC1778) and non-reactive coarse aggregate were used for the research presented herein. The Jobe-Newman fine aggregate was from El Paso, Texas. The fine aggregate has been classified as one of the most reactive fine aggregates in the United States (Phillips et al., 2015). Concrete cubes were cast using a pavement mix-design. After an initial curing period, external uniaxial and biaxial restraint was applied to each specimen. The restraint stresses were applied to the concrete cubes and then the cubes were stored at 38ºC and 95% RH for 6 months to accelerate ASR formation and expansion. A similar load application method as the one developed by Bishnu (2015) and Gautam and Panesar (2015) was adopted in this research. ASTM C1260 and ASTM C1293 standard test were carried out to determine the reactivity of the aggregate. The DRI method was used to evaluate the development of deterioration and cracking within the concrete.

3.2. Cements

A high-alkali (0.84% Na_2O_{eq}) cement that complies with ASTM C150 and AASTHO M85 was used in all the experiments. It was supplied from Lehigh Heidelberg Cement Group. The chemical properties, as provided by the manufacturer are summarized in Table 3-1.

Table 3-1 Chemical composition of cement.

Constituents	**CaO**	**SiO_2**	**Al_2O_3**	**Fe_2O_3**	**SO_3**	**MgO**	**C_3S**	**C_3A**	**Total Na_2O_{eq}**
Percentage	62.38	20.06	5.21	3.01	3.43	2.21	52.42	8.70	0.84

3.3. Aggregate

Aggregate is the major component of concrete, which influence its mechanical properties. Hence, the properties of aggregate can affect those of concrete. In this study, reactive fine aggregate and non-reactive coarse aggregate were used.

The source of reactive fine aggregate used in the study was from EL Paso, Texas. The sand is mainly composed of quartz, feldspars, siliceous volcanic phases and chert. The Jobe-sand expanded between 0.5% and 0.59% in the 14-day accelerated mortar bar test (Phillips et al, 2015; Thomas et al., 2006). The non-reactive coarse aggregate was a 3/4 in. crushed limestone from Youngstown, Ohio.

3.4. Aggregate Grading and Concrete Mix Design

Although the ASTM C1293 mixture design has become a standard for ASR research, a pavement mix design was adopted for the testing done herein. The mixture design used a typical FHWA cement content of 564 lb/yd^3 (335 kg/m^3) to better represent the mechanical properties of concrete pavement. The water-to-cement ratio was 0.47. The reactive fine aggregate and coarse aggregate were used in the natural gradation. The alkali content of concrete mixture was increased from 4.74 lb/yd^3 (2.81 kg/m^3) to 7.05 lb/yd^3 (4.18 kg/m^3) by adding NaOH pellets to the mixing water. The mix design for the cube specimens is summarized in the Table 3-2.

Table 3-2 Mix-design for concrete cube specimens.

Material	Cement	Rock	Sand	Water
Weight lb/yd^3	564	1850	1317.8	265.08
Weight kg/m^3	335	1098	782	157

3.5. Formwork

The formwork was designed specifically for casting 10 in (254 mm) cubes with embedded studs for measuring strain. A 0.75 in. (19 mm) thick plywood was used to make the formworks. The precisely cut plywood pieces were joined together using glue and screws. A total of 3 sets of formwork were constructed. The detachable formworks were then re-used to produce a total of 9 cubes. The wooden formwork is shown in the Figure 3-1. The formworks were made with four 5/32 in. (4 mm) diameter holes for placing the strain measurement studs. The studs were placed 6 in. (150 mm) on center to align with the detachable-mechanical strain gauge (DEMEC). Four lager holes of 0.5 in. (12.5 mm) diameter were drilled into two opposite faces for placing the sheaths and post-stressing rods.

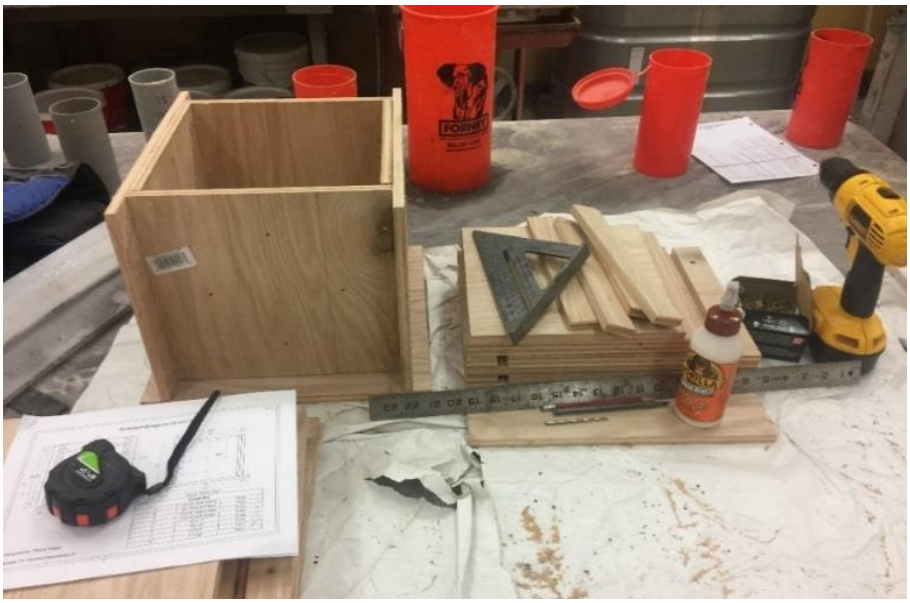

Figure 3-1 Construction of wooden formwork for 10 in. concrete cubes, with holes for strain measurement studs.

3.5. Expansion Measurement Studs

The strain due to ASR in the concrete cube specimens was measured using the embedded studs and detachable-mechanical DEMEC gauge as shown in the Figure 3-2 (a). Four studs

were installed in the three mutually perpendicular planes (X, Y, and Z) to measure expansion. The brass studs were embedded 1 in. (25 mm) into the concrete and the gauge length for the expansion measurement was set to 6 in. (150 mm) A stud was attached to the formwork by use of a screw as shown in the Figure 3-2 (b). During demolding, the screws were removed first, followed by the removal of the formwork. This process allowed the studs to remain embedded into the concrete cube. These studs were flush with the exterior concrete surface. Hence, a DEMEC gauge was used to measure the change in distance between each a pair of studs.

The DEMEC gauge has a 0.6 in. (15 mm) range with a resolution of 0.0001 in. (0.0025 mm) The DEMEC gauge was zeroed to the standard invar reference bar (6.0000 in. [150 mm]) before measurements of each specimen. The initial measurements were taken before the cubes were stored in conditions to accelerate ASR. Strain was subsequently calculated as the difference between the length-change at each measurement and initial length-change divided by the reference length (6 in. [150 mm]).

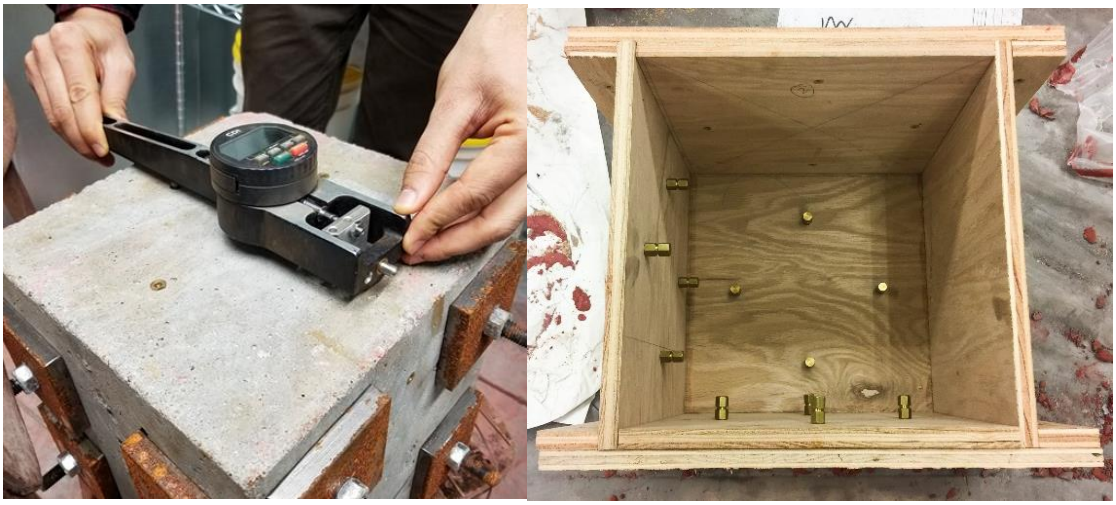

Figure 3-2 (a) DEMEC gauge used for the expansion measurement of the cubes. (b) Placement of expansion measurement studs in the formwork.

3.6. Sheaths

Stainless steel tubes of inside diameter 0.7 in. (18 mm) and wall thickness of 0.083 in. (2.1 mm) were used as sheaths to allow later application of the post-stressing rods. Each 6 ft. tubes was cut into 9.5 in. of long pieces. Since any interior space in the concrete undergoing ASR may reduce the expansive pressure, there should not exist any empty volume within the concrete. Therefore, a rigid tubes of 0.083 in. wall thickness were selected to resist pressure from the reaction in the concrete.

The specimen undergoing uniaxial restraint were cast with four sheaths (along a single axis, Figure 3-4) whereas specimen undergoing biaxial stress were cast with eight sheaths (four along each perpendicular axis, Figure 3-5). The sheaths diameter were chosen carefully so as to provide enough room between the post-stressing rod and the sheath to aid the free movement of a rod fixed with a strain gauge. The tubes were cut 0.5 in. shorter than the 10 in. cube to prevent stress transfer from the plates into the tubes. The steel sheathes were placed in the formwork using small plastic tubes as shown in the Figure 3-3. These especially made plastic tubes were removed before demolding the formwork.

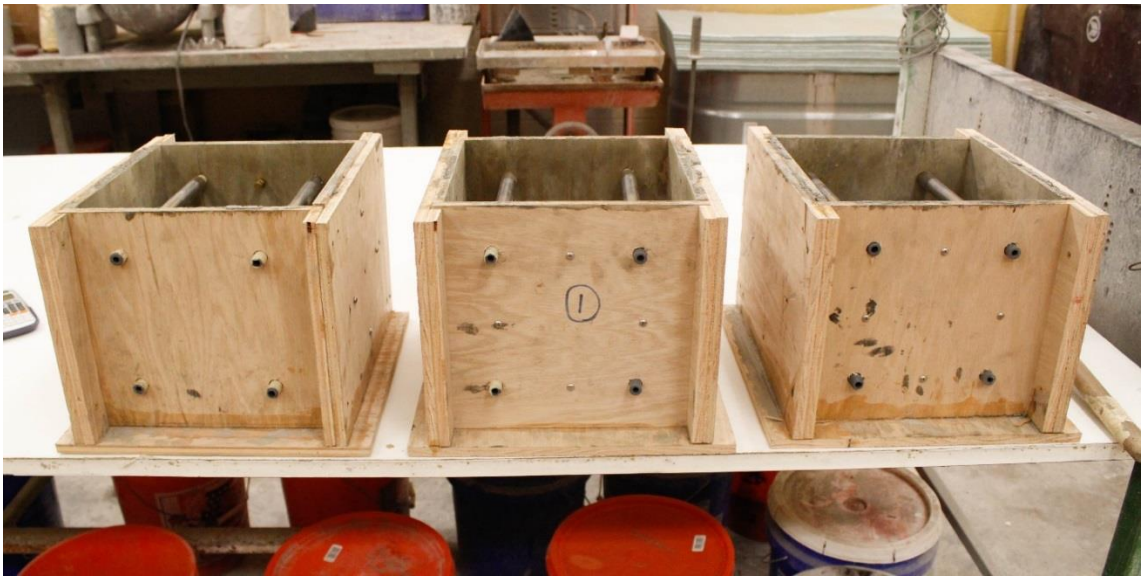

Figure 3-3 Placement of steel sheathes using plastic tubes.

3.7. High-Strength Bolt

High-strength Class 10M threaded bolts were used to post- tension the cubes along one or two axis. Based on the design, 0.5 in. (Appendix A) identical bolts were used for all the cubes. Each 39 in. long thread bolt was cut into 14 in. length pieces. The main reason behind choosing Class 10M rod was the high strength and ductility, and the similar thermal expansion coefficient to that of the concrete specimen used in this research. The stainless steel sheaths were used to prevent rusting and corrosion. Class 10M has a yield strength of 130,000 psi and a tensile strength of 145,000 psi. A tension test was preformed to determine the actual strength of the threaded bolt. Grade 10M, 0.5 in. hex nuts were used to tighten the bolts.

3.8. Bearing Plate

High-strength ASTM 108 1018 alloy steel base plates were used with the threaded bolts to apply confining stress to the concrete cubes. Based on the experimental design, the required minimum thickness for the base plate was 0.288 in. and the minimum size was calculated to be 2.1 in. x 2.1 in. (Appendix A). However, the thickness of 0.5 in. and size of 3 x 3 in. were selected to remain on the conservative side. The carbon steel plates came with the dimension of 1/2 x 3 in x 1 ft. and were cut to 3 in. x 3 in. A 3/5 in. diameter hole was then drilled into the center of each plate for the post-tension bolts.1018 steel base plates were chosen because of good ductility, toughness and strength qualities. 1018 steel plate has tensile strength of 65,000 psi and yield strength of 55,000 psi.

3.9. Casting of Specimens

To investigate the effects of uniaxial restraint, biaxial restraint, and unrestrained concrete in ASR expansion, 9 concrete cube specimens were cast. The confining stresses are

summarized in Table 3-3. Three identical cube specimens were cast for each of the three stress states. For each batch of concrete, three 4 x 8 in. cylinders were cast for determination of compressive strength and modulus of elasticity at different age. Similarly, for each stress state, three replicates were cast.

The concrete cubes were batched at the YSU Concrete Materials Lab, at a controlled temperature of 72º F. Each mixture was weighted out as two separate batches as shown in Figure 3-6 below. The NaOH was added to the mixing water and mixed until dissolved. Each mixture was batched and then combined and mixed by shovel to produce a single 2.2 ft^2 mixture.

Figure 3-4 Preparation of formwork before batching uniaxial concrete cubes.

Figure 3-5 Preparation of formwork before batching biaxial concrete cubes.

Figure 3-6 Concrete mix-design preparation before batching.

The casting process involved, first placing the forms on a level surface. The inner surface of the molds were then lubricated using WD-40 to prevent the bonding between mold and concrete. Second, the concrete was placed in the mold by distributing evenly around the mold using a scoop. The concrete was placed in 3 equal layers. Third, each layers of concrete were tamped 25 times evenly using tamping rod and the sides of the mold were gently tapped 5-8 times using mallet as shown in the Figure 3-7. Fourth, the top of the concrete was leveled off with a trowel to produce an even and level surface. The concrete cylinders were cast and stored accordance with the requirements of ASTM C31. Finally,

the concrete cube specimens and cylinder were stored at a room temperature and demolded 1 day after casting.

Figure 3-7 Compacting the concrete using a tamping rod.

3.10. Loading and Conditioning of Specimens

3.10.1. Strain gauge

The confining stress was applied to each specimen through the post-tensioning bolts. The strain in the threaded bolt during posttensioning was monitored using a strain gauge and digital indicator. Strain gauges (from Omega Engineering, Inc.), with resistance of 120.4 Ω ±0.35%, gage factor 2.05±1.0%, transverse sensitivity of -0.1%, and integrated wire, were attached at the center of each threaded rod. The center of each rod was machined to remove the threading, and cleaned properly with a towel. Then, a strain gauge was glued using the instant adhesive as shown in the Figure 3-6 (b). Grooves were cut into the surface of the cubes to pass the strain gauge wire under the bearing plates. A diamond saw blade was used to cut grooves in the specimens. Finally, the wire was covered with a tape so that it would not be cut by the bolts during posttensioning. One strain gauge was used for uniaxial cubes where as two gauges were used for biaxial cubes. The Model P3 Strain

Indicator and Recorder was used for monitoring the strain in the bolts during loading. The strain gauge was connected to the P3 and load application was monitored during the process as shown in the Figure 3-8.

Figure 3-8 (a) Strain monitoring of the rod using P3 Strain Indicator. (b) A strain gauge glues on the rod using the instant adhesive.

3.10.2. Loading

The confining stress was applied to the concrete cubes at an age of 2 months after casting. The bolts were hand tightened first and the strain gauge wire was passed through the groove and underneath the bearing plates. A torque wrench and socket were used to tighten each bolt to the necessary torque.

Numerous trail stress application were performed and target strain of 4000 microstrains and 3000 microstrains were made initially for 435 psi (3 MPa) and 363 psi (2.5 MPa) stress state cubes respectively. The torque was calculated to be 87.067 lb.ft and 67.68 lb.ft to achieve strain of 4000 microstrains and 3000 microstrains respectively. The torque wrench was set to the calculated value and the load was applied to the bolt one at a time until the required strain was achieved.

Table 3-3 Detail of confining stress applied to the cubes.

Type	Confining Stress (psi)			Total
	X- Axis	Y-Axis	Z-Axis	
Unrestraint	0	0	0	3
Uniaxial Restraint	435	0	0	3
Biaxial Restraint	0	435	363	3
Total Cubes				9

3.10.3. Conditioning

The specimens were cured at room temperature (23) from demolding until 56 days. They were stored in curing tank over water, but not in contact with the water. This provided a moist environment without allowing alkalis to leach from the samples. After 2 months of curing, the cubes were relocated to warm room as shown in the Figure 3-9. The temperature and relative humidity inside the chamber was maintained at 38±2ºC and >95%, respectively.

Figure 3-9 Cube specimens being cured inside accelerated chamber.

3.9. Test Details

3.9.1. Cubes

The concrete cubes were measured periodically for change in strain. The initial reading for strain was taken at the age of 2 months after casting, before moving the specimens to the environmental chamber. After 4 months in environmental chamber, one cube each from unrestraint, uniaxial and biaxial restraint state were examined using the DRI method. Each larger cubes were then cut using diamond blade into eight smaller 5 x 5 in. cubes.

The DRI was analyzed on four smaller cubes from each different stress state and the other four smaller cubes were left for later use. For each larger cubes, four smaller cubes which from diagonally opposite octant to each other were taken and polished for examination under a digital microscope. Each smaller cubes had three different planes namely XX, YY and ZZ. The DRI value for concrete for three different planes were obtained as the average from four cubes from one larger cube.

The value obtained from DRI test was then used for choropleth mapping of the damage in three different planes of concrete cube specimens. The color scale of red, yellow and green was used to indicate the extent of damage in the concrete. This mapping technique is useful in locating the area according to scale of damage.

3.9.2. Prisms

The CPT and AMBT were carried out in accordance with ASTM C1293 (ASTM C1293, 2008) and ASTM C1260 (ASTM C1260, 2001). The grading and mix design for both of the test are summarized in the literature review. The prisms for CPT test were condition at 38°C and 100% RH. The strain measurement were taken at 7, 28, 56, 90 and 180 days. The result of six month of strain measurement is highlighted in Appendix C.

Similarly, two different fine aggregate were tested for reactivity using AMBT. Usually this test is 16 days long but we extended the test for total of 28 days for better outcome. The results from the AMBT are summarized in Appendix B.

3.9.3. Cylinders

Cylinders were casted for determining modulus of elasticity and the compressive strength. The concrete cylinder specimens were tested for modulus of elasticity in accordance to ASTM C469 (ASTM C469, 2014) and compressive strength in accordance with ASTM C39 (ASTM C39, 2001). The cylinders were conditioned at room temperature from day of demolding to an age of 2 months. They were tested to determine modulus of elasticity and the compressive strength at the age of 28 day. The result of the tests are summarized in Appendix D.

Chapter 4 Result and Discussion

4.1. Introduction

This research project involved monitoring the axial distribution of ASR-induced expansions in nine 10 in. (254 mm) concrete cube specimens, three concrete cube specimens of each stress state unrestraint, uniaxial and biaxial. The concrete specimens were restrained with 435 psi (3 MPa) and 363 psi (2.5 MPa) of confining stress. The reactivity and expansion of unrestrained concrete prism were monitored using the AMBT and CPT in accordance with ASTM C1260 and ASTM C1293 respectively. The cube specimen strain due to ASR were measured using the embedded studs and DEMEC gauge. The cube specimens were stored at 38°C and 98% RH for accelerating the rate of ASR and strains were monitored every week. The strain data collected were averaged and analyzed for x, y and z axes. The strain measurement in concrete cube specimens are considered to be the accumulation of all the thermal, shrinkage, and expansive chemical strains by ASR. After four months in the environmental chamber, the cubes were analyzed using DRI method for investigating the internal damage due to ASR. Furthermore, the damage mapping of three different planes (i.e. x, y, z) was done using the DRI data for the better understanding of the damage in the concrete. Mechanical properties such as compressive strength and modulus of elasticity were also documented over the course of the research period.

4.2. Prism Expansion

The free expansion of concrete prism was measured in accordance with ASTM C1293. The studs acted as measurement points for measuring the length change. Prism measurement were taken relative to a steel reference bar using a micrometer as shown in the Figure C-1.

Six prisms were cast with same concrete mix design (Table 2-3). The average free expansion of prism using the Jobe sand showed rapid expansion development over the first 56 days before beginning to slow and peak at 0.266% and 0.358% (Figure 4-1). The CPT is a yearlong test, but only six month of readings were completed due to time resistant. Although the peak value for the expansion is expected to increase over time. The expansion exceeded the CPT threshold of 0.04% within 10 days.

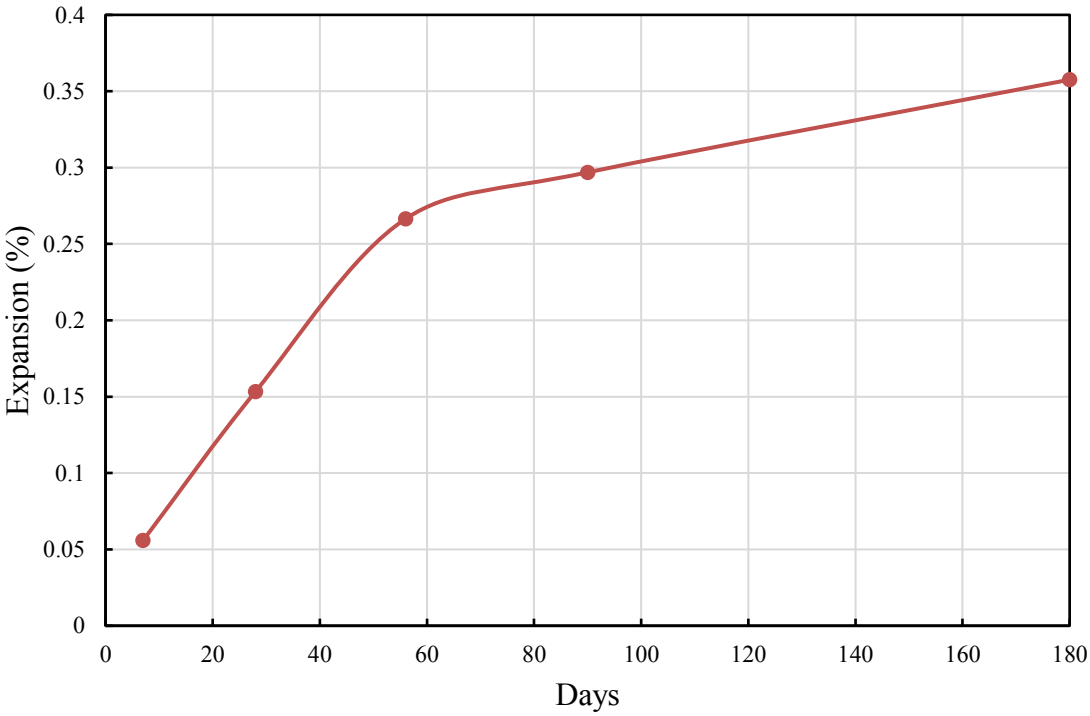

Figure 4-1 Expansion of Jobe sand in the concrete prism test as per ASTM C1293.

4.3. Mortar Bar Expansion

The reactivity of the Jobe sand and normal sand is tested using a mortar bar in accordance with ASMT C1260. The test result is shown in the Figure 4-2 and Figure 4-3. As shown in the Figure 4-2, the expansion was 0.36% at 14 days and 0.49% at 28 days for Jobe sand. From Figure 4-3, expansion for the normal sand was 0.09% at 14-days and 0.21% at 28 days. Since, the expansion was greater than 0.1% at 14-days for Jobe sand, it confirms the sand as reactive.

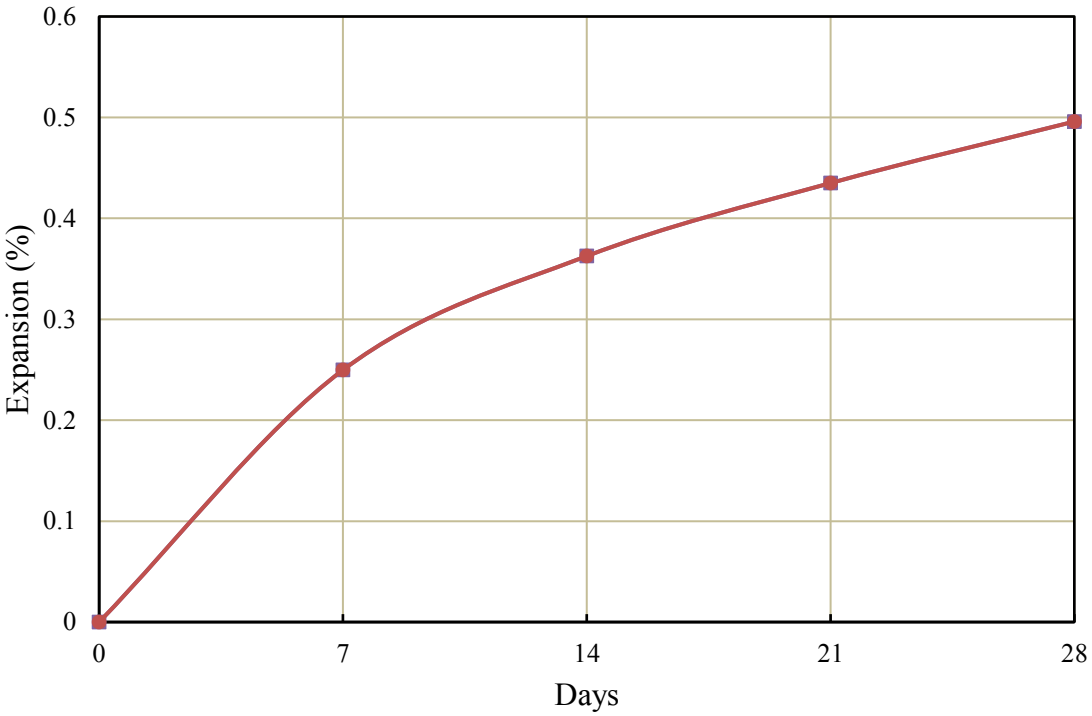

Figure 4-2 Expansion of Jobe sand in the accelerated mortar bar test as per ASTM C1260.

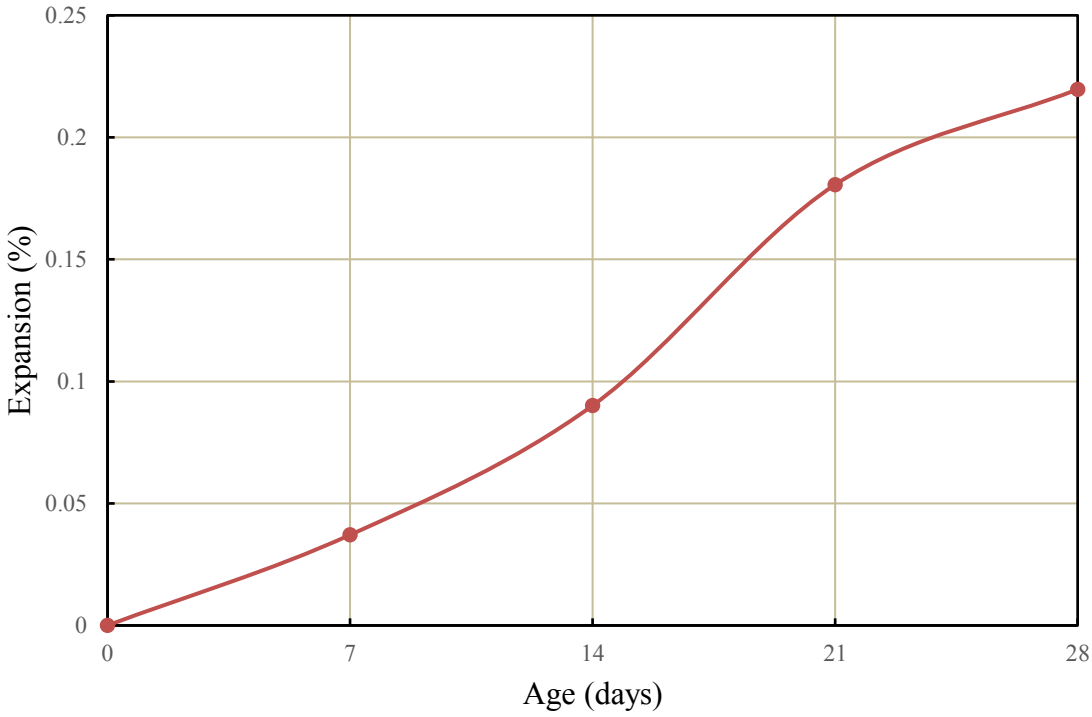

Figure 4-3 Expansion of non-reactive sand in the accelerated mortar bar test as per ASTM C1260.

4.4. Cube Expansion

The development of axial and volumetric expansion over time due to ASR was documented and analyzed in this research. The reported expansions for different stress state represent the average of the strains measured in three cubes in three different planes (i.e. x, y, z). The variability in the strain measurement may have been due to measurement errors, environmental errors and ASR expansion. The strains measured on reactive concrete cube specimens with uniaxial and biaxial applied loading have been compared to measurement with free expansion on concrete prism and free expansion on concrete cube specimens.

The evolution of axial, ultimate and volumetric expansion in different stress state cube specimens are presented in the Figure 4-1 through Figure 4-8. Figure 4-4 shows the evolution of expansion in three direction X, Y and Z where all the directions are unrestrained. Similarly, Figure 4-5 shows the expansion of uniaxial specimen where only

X direction is restrained and Figure 4-6 shows the expansion of biaxial specimen where X direction is unrestrained and Y and Z directions are restrained. It can be noted that, the specimens underwent negative strain at approximately 15 days of post tensioning. This concrete shrinkage may be due to the pressure applied during the post tensioning. At approximately 40 days after curing inside the environmental chamber, there was a relatively abrupt shift in expansion behavior for the concrete cube specimens (Figure 4-4, Figure 4-5 and Figure 4-6). Expansion rates were found to be increasing. This may be because of formation of ASR. After 4.5 months, axial expansion in unrestraint specimens remained in the range of 0.24-0.25% while those in uniaxial and biaxial stress remained in the range of 0.12-0.24% and 0.09-0.23% respectively.

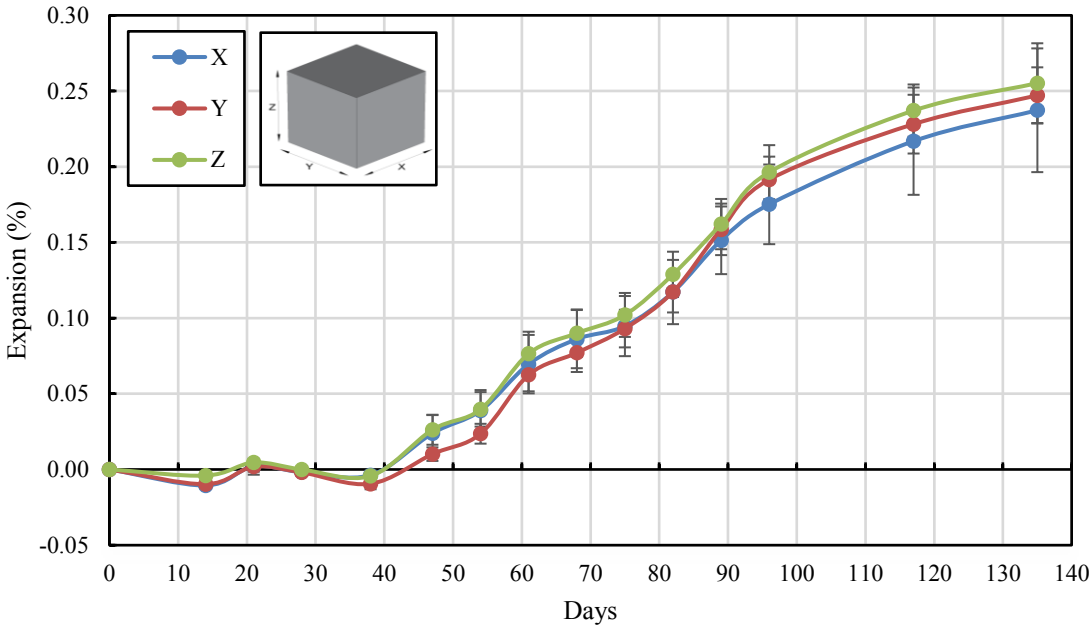

Figure 4-4 Evolution of axial strain of the unrestraint cube specimen in x, y, and z plane.

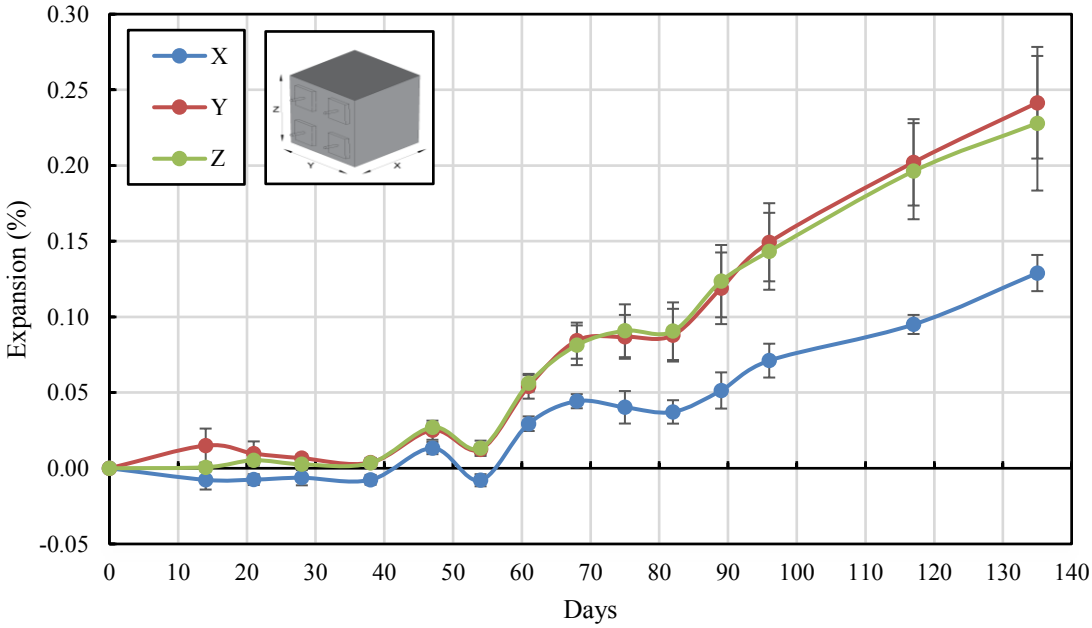

Figure 4-5 Evolution of axial strain of the uniaxial cube specimen in x, y, and z plane.

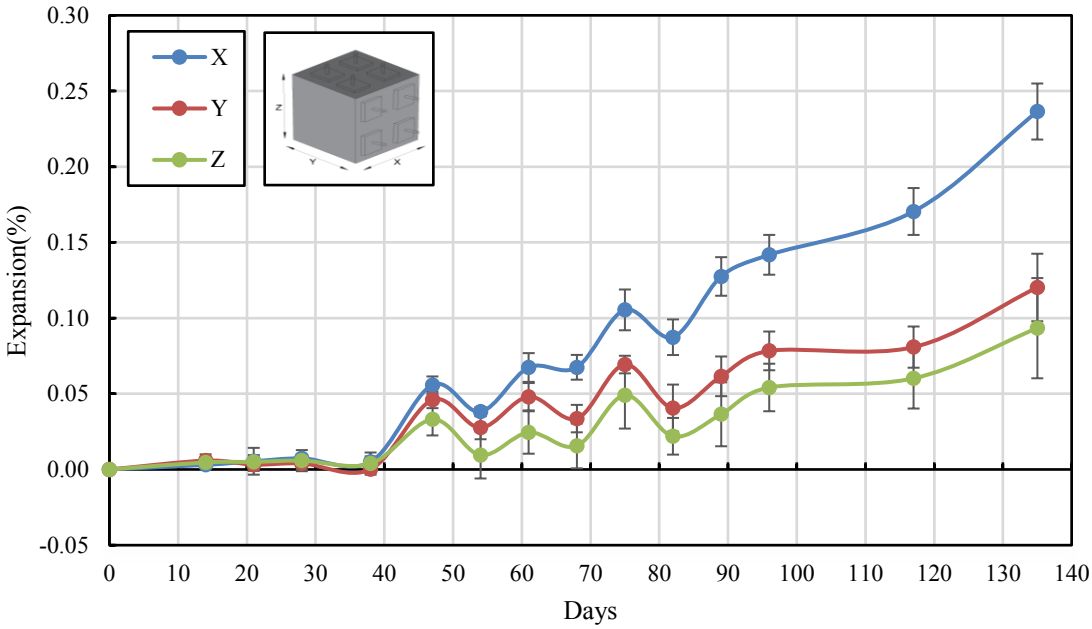

Figure 4-6 Evolution of axial strain of the biaxial cube specimen in x, y, and z plane.

The unrestrained, uniaxial and biaxial stress state specimens exhibited similar expansion in unrestrained directions with minor variation, as seen in Figure 4-7. However, the expansion was lower in restrained planes of the uniaxial and biaxial. The results in Figure 4-7 show that the expansion due to ASR was significantly affected by the stress state. For instance, in unrestrained specimens, expansion in all direction was identical. Whereas in uniaxial specimens the expansion was reduced in the X direction with similar expansion in other two directions. Similarly, for biaxially restrained specimens, the expansion was greatly reduced in both the stressed direction (Y and Z), and greater expansion was observed in the unrestrained direction (X). These observation indicate that the expansion was reduced in the presence of stress and expansion was transferred to unrestrained direction. These result are similar to the results concluded in the paper published by Gautam (2016).

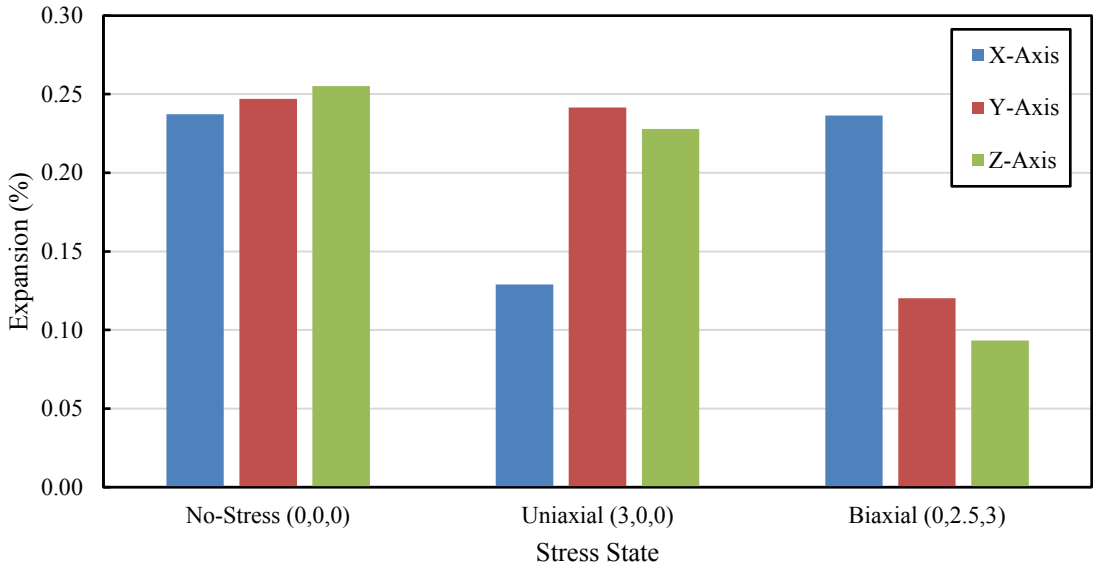

Figure 4-7 Ultimate strain of cube specimen with different stress state.

The total ASR expansion result for all stress state specimens are presented in Figure 4-8 below. The volumetric expansion remained fairly constant till an age of 40 days than for the consecutive ages. The total expansion due to ASR in the unrestrained state was relatively larger than that in uniaxial and biaxial concrete cube. The volumetric expansion was reduced by 20% for uniaxially restrained specimens and 40% for biaxially stressed specimens. From the above inspection, it can be concluded that total volumetric expansion is reduced by restraint, which was the opposite of what was observed by Gautam (2016).

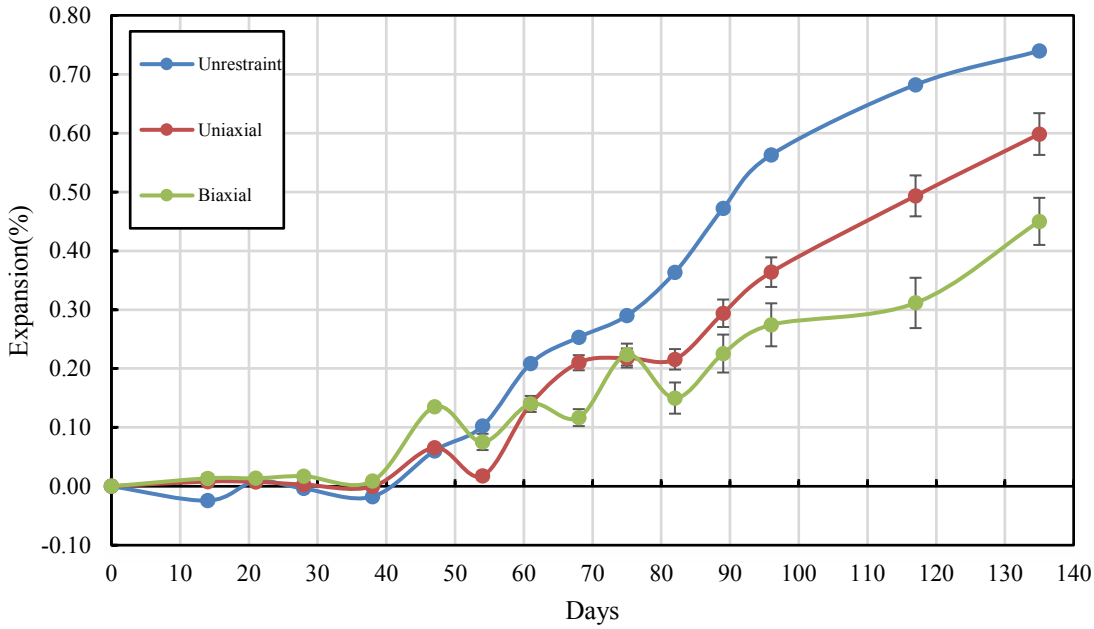

Figure 4-8 Change in volumetric expansion of cube specimens with different stress states.

4.5. DRI for three different stress state

The DRI values for the reference cylinder specimen tested at the age of 3 months was 423. The DRI values for the concrete cube specimens corresponding to the three stress state at 4.5 months of accelerated curing in presented in Table 4-1.

It can be noted, that the extent of the damage varied with different stress state but the ASR was not prevented by the stresses. As shown in Table 4-1, the DRI value for the uniaxially and biaxially loaded specimens are about 42% and 38% lesser than the DRI value for the unrestrained specimen measured at the same age.

Table 4-1 DRI values for different cube specimens.

Stress State	Planes	DRI Value	Average DRI Value
Unrestraint	XX	643	711
	YY	756	
	ZZ	733	
Uniaxial	XX	431	410
	YY	419	
	ZZ	380	
Biaxial	XX	451	442
	YY	439	
	ZZ	435	

Figure 4-9 through Figure 4-11 shows the contribution of the various damage features to the DRI value of the specimens for all the stress states for XX, YY, and ZZ planes at 4.5 months of accelerated curing. Figure 4-9 shows the DRI value for the unrestrained cube specimen along three mutually perpendicular planes XX, YY and ZZ. DRI value for the features like closed cracks in aggregates (CCA), open cracks in aggregates (OCA), coarse aggregate debonded (CAD), disaggregated aggregate particle (DAP) and cracks in cement paste (CCP) seems to be similar for all three planes. Since, all the planes are unrestrained and expansion in all three planes are similar, damage due to ASR transferred equally in all direction. It can be noted from Figure 4-9 that the small numbers of open cracks in aggregate and cement paste with presence of ASR gel can be seen on all the planes for unrestrained specimens. This observation shows the progression of ASR reaction with increasing expansion.

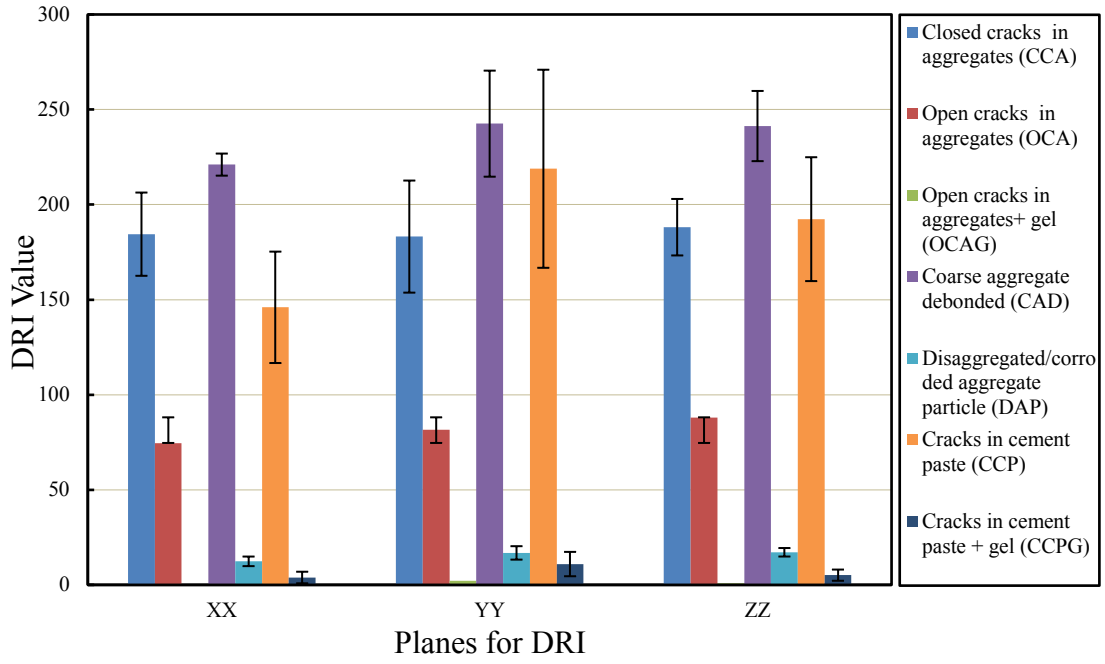

Figure 4-9 DRI values along the three planes of the unrestraint cube specimens.

Figure 4-10 represents the DRI values along the three planes of the uniaxial cube specimens with XX-plane restrained. DRI features like CAD and CCP in uniaxial specimens is 51% and 113% respectively lesser than compared to unrestrained specimens but in case of CCA which is 15% higher in uniaxial specimen. Similarly, From Figure 4-11 it can be observed that CAD is 58% and CCP is 87% lesser than that of unrestrained specimens but CCA is 25% higher in biaxial specimens. This shows that the stress reduces the opening of crack perpendicular the direction of stress, similar to what was observed by Gautam (2016). In addition, the coarse aggregate debond and cracks in cement paste increase in the counts with increasing expansion. There are no evidence of ASR gel in aggregates as well as in cement paste in both uniaxial and biaxial cube specimens.

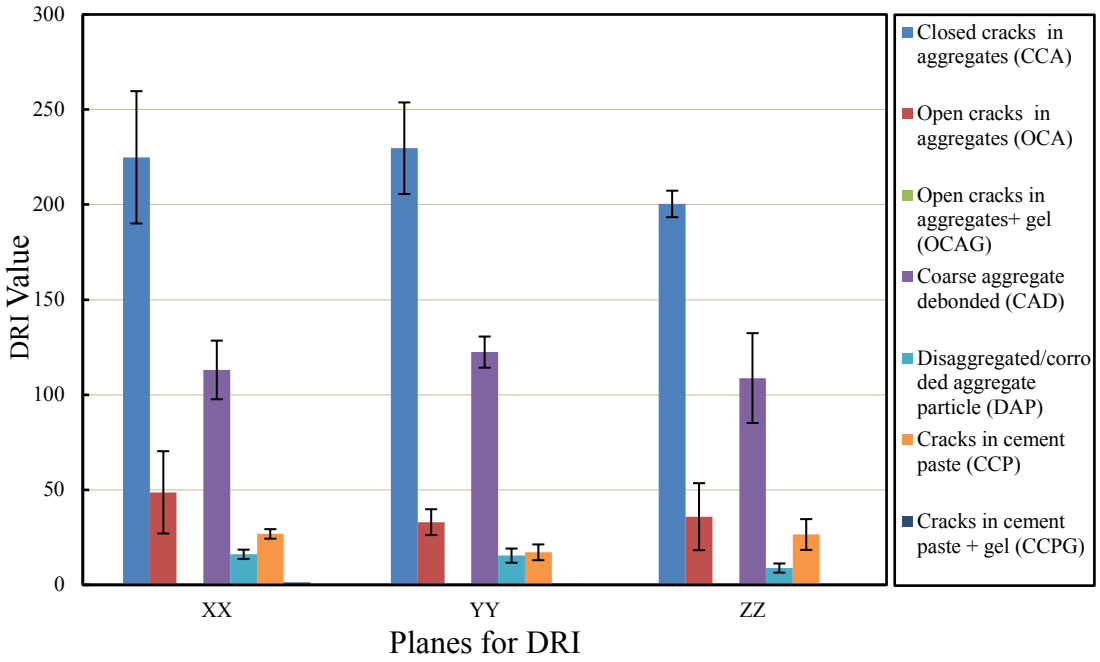

Figure 4-10 DRI values along the three planes of the uniaxial cube specimens.

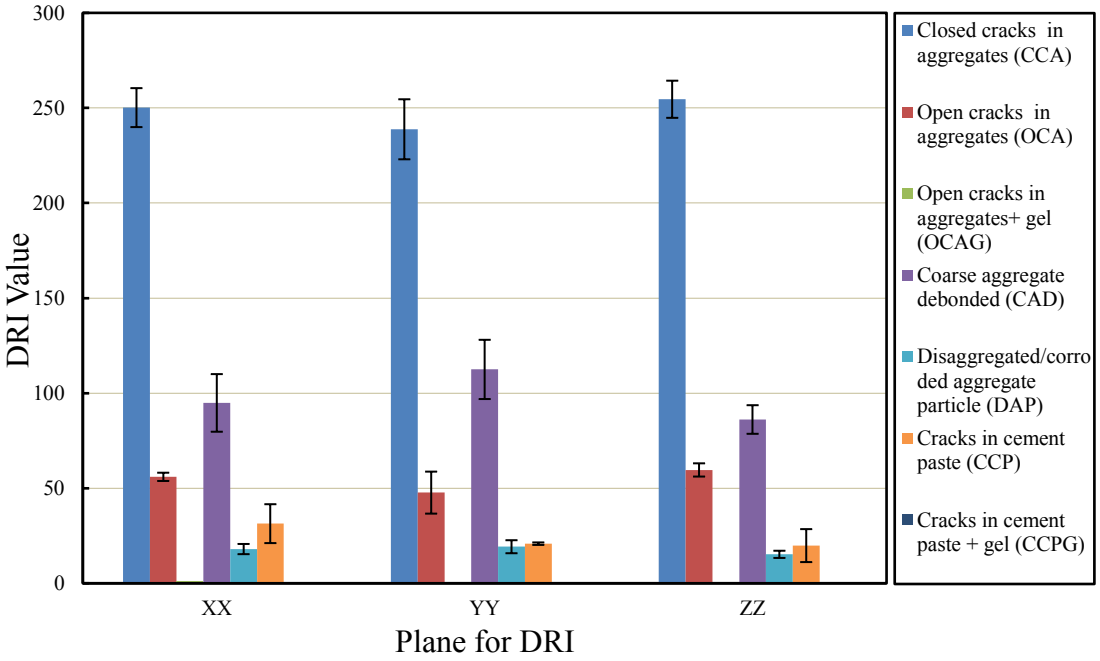

Figure 4-11 DRI values along the three planes of the biaxial cube specimens.

Figure 4-12 shows the comparison of DRI values between three different stress states. From the study done by Sanchez et al. (2014) it is concluded that the DRI value the increase

linearly with increasing expansion. But from Figure 4-7 and Figure 4-12, DRI values of different planes of different stress state cube specimens does not seem to correlate well with the expansion levels. For instant, expansion in X-direction of uniaxial specimens is only 0.13% which is much lesser than in other two directions but the DRI value is 431 which is higher than for Y and Z direction. In contrast, DRI value in unrestraint specimens seems to increase with increasing expansion. This might me due to the limited number of specimens that were tested in this study. Thus, the DRI value of the concrete cube specimens of three different stress state shows that the stress are unlikely to stop ASR, but may still be effective in reducing the ASR damage of concrete.

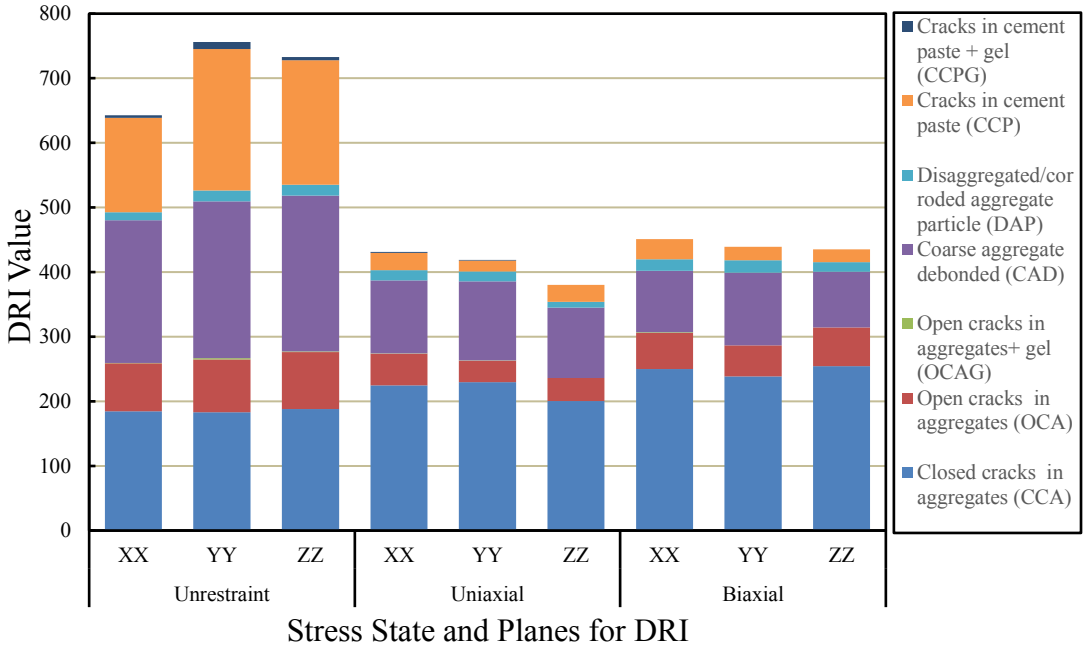

Figure 4-12 Comparison of DRI values along the three planes of three different concrete cube specimens.

4.6. DRI Mapping

DRI mapping of different planes of concrete cube specimens was done using the value obtained from DRI test. The seven features of the DRI test were counted carefully under

the microscope and values of DRI were plotted in each grid of corresponding planes (i.e. x, y, z). Choropleth mapping was used to summarize the extent of damage due to ASR in the concrete cube. The color scale of red, yellow and green was used for the mapping. The red indicates maximum DRI value, yellow indicates midpoint DRI value while green indicates minimum DRI value. Figure 4-13 through Figure 4-21 presents the damage mapping for the concrete cube specimens corresponding to the three stress state at 4.5 month of accelerated curing.

Figure 4-13 through Figure 4-15 shows the damage mapping along the three mutually perpendicular planes XX, YY and ZZ of unrestraint specimens. It shows that the DRI value is relatively larger in the mid area than in the boundary area of the cube specimens which indicates that the damage due to ASR in that area is higher in mid area. These observations also shows the degree of damage in the unrestraint specimen in all three planes are even distributed with smaller variation in XX-plane.

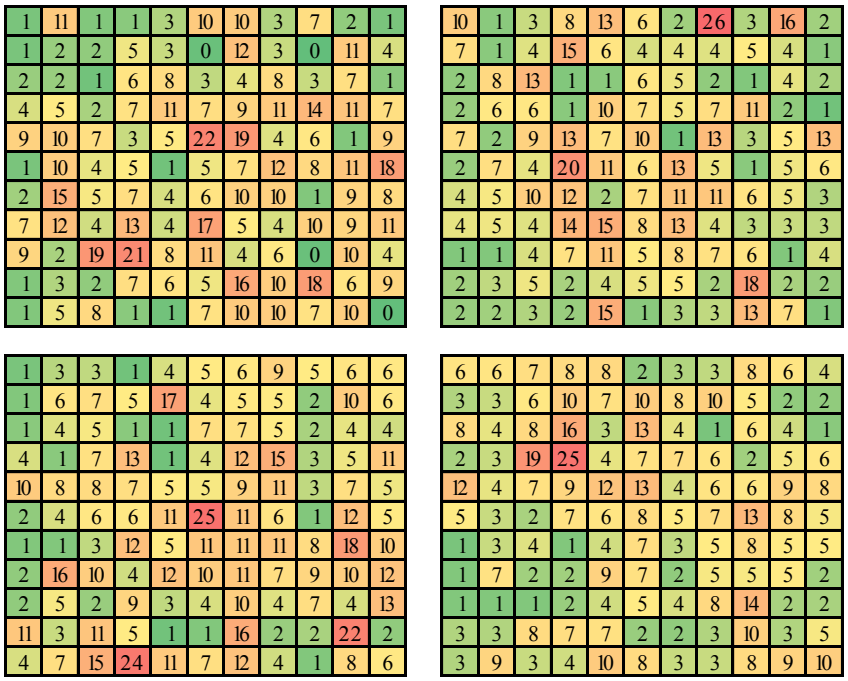

Figure 4-13 Damage mapping of XX-plane of unrestraint specimen.

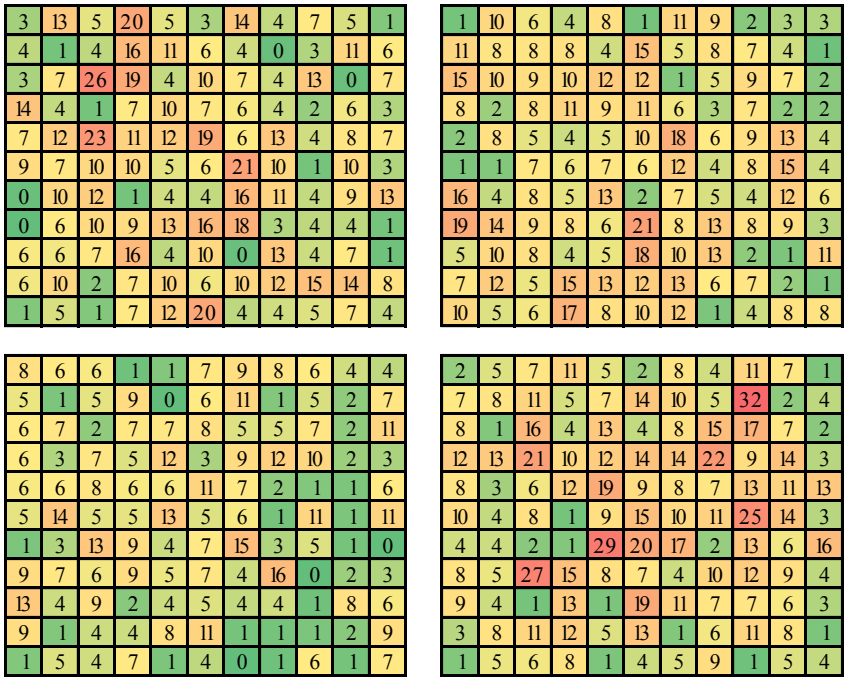

Figure 4-14 Damage mapping of YY-plane of unrestraint specimen.

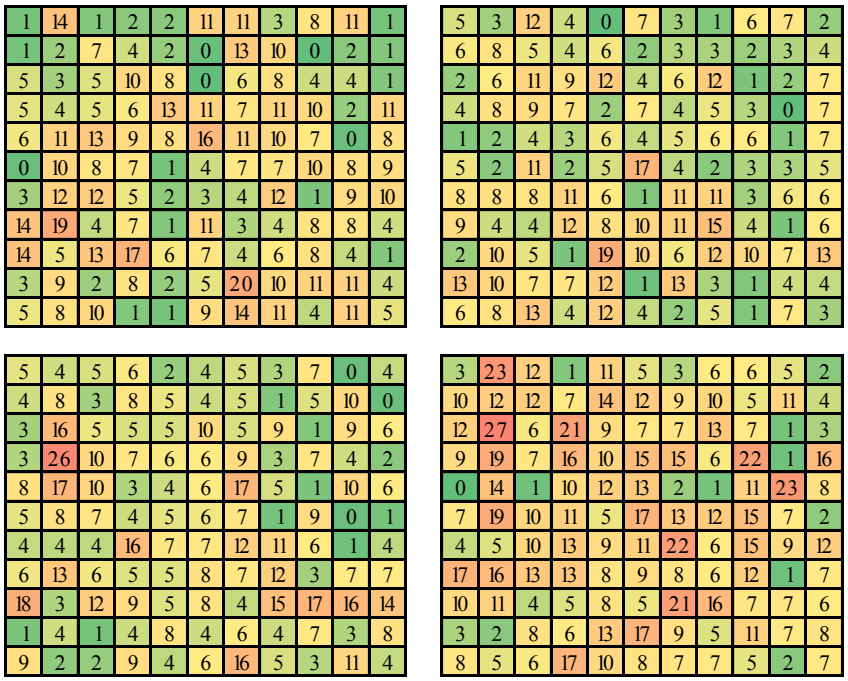

Figure 4-15 Damage mapping of ZZ-plane of unrestraint specimen.

Figure 4-16 through Figure 4-18 presents the damage mapping of uniaxial concrete cube specimens. The blue circle in the map indicates the positon of rod for stress application. From the damage mapping it can be noted that the degree of damage in uniaxial specimens seems to be considerably lesser than that of unrestraint specimens. Figure 4-13 through Figure 4-15 shows the damage mapping along the three mutually perpendicular planes XX, YY and ZZ of biaxial specimens.

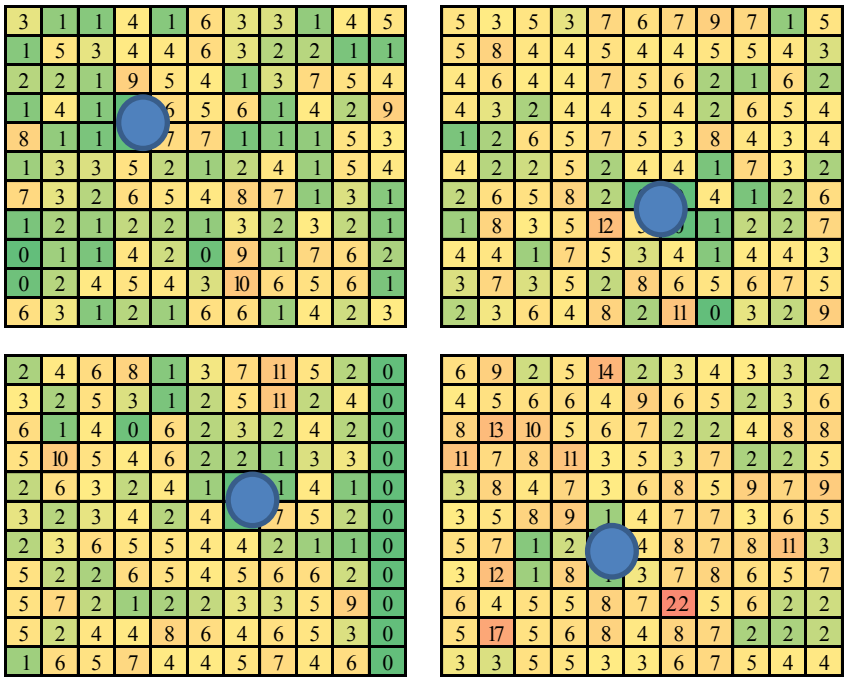

Figure 4-16 Damage mapping of XX-plane of uniaxial specimen.

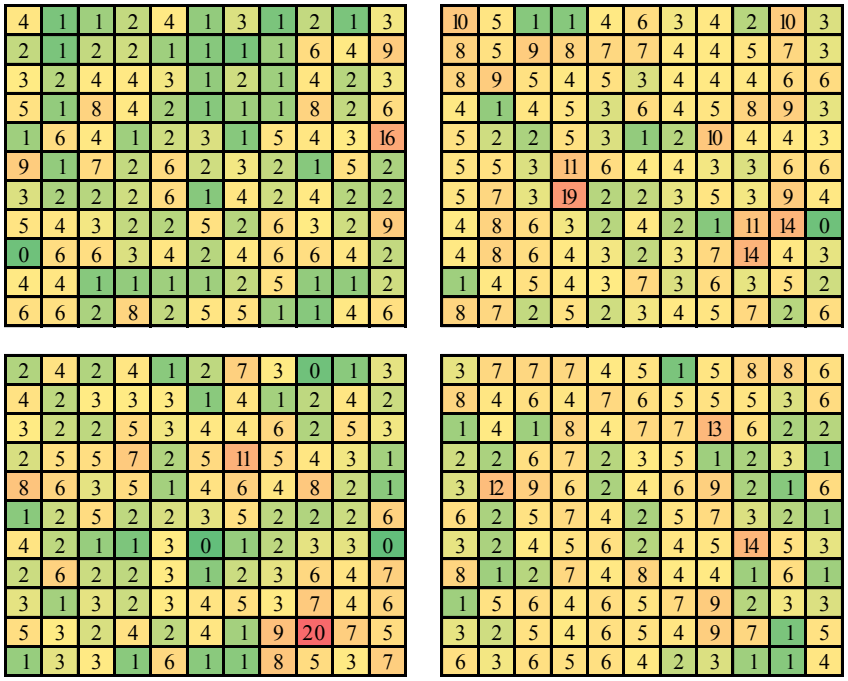

Figure 4-17 Damage mapping of YY-plane of uniaxial specimen.

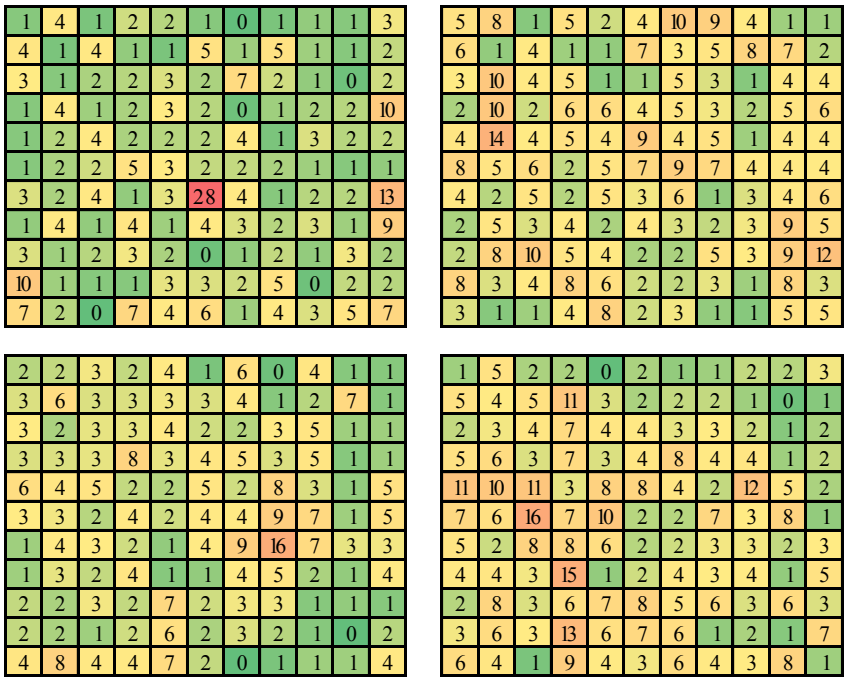

Figure 4-18 Damage mapping of ZZ-plane of uniaxial specimen.

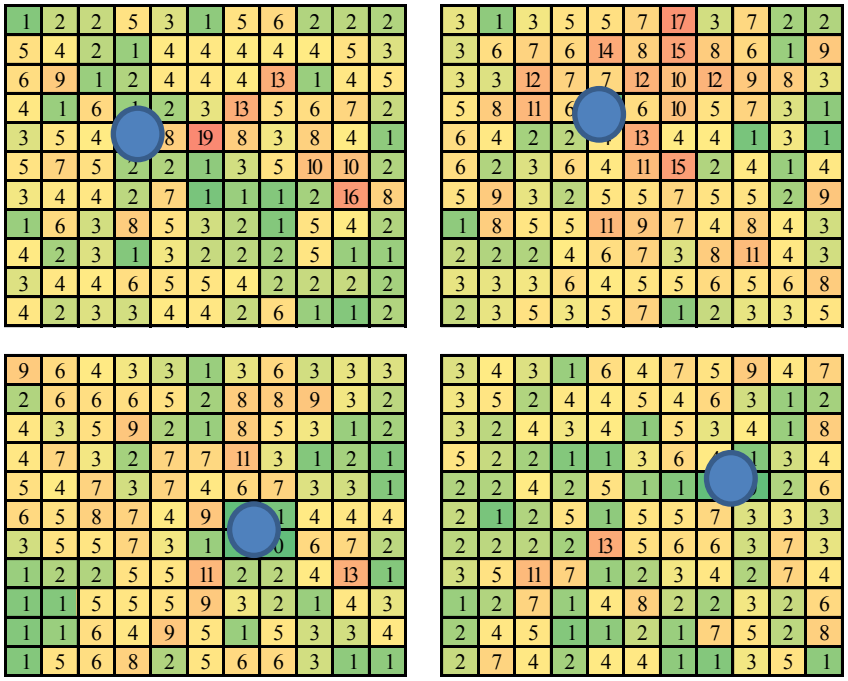

Figure 4-19 Damage mapping of XX-plane of biaxial specimen.

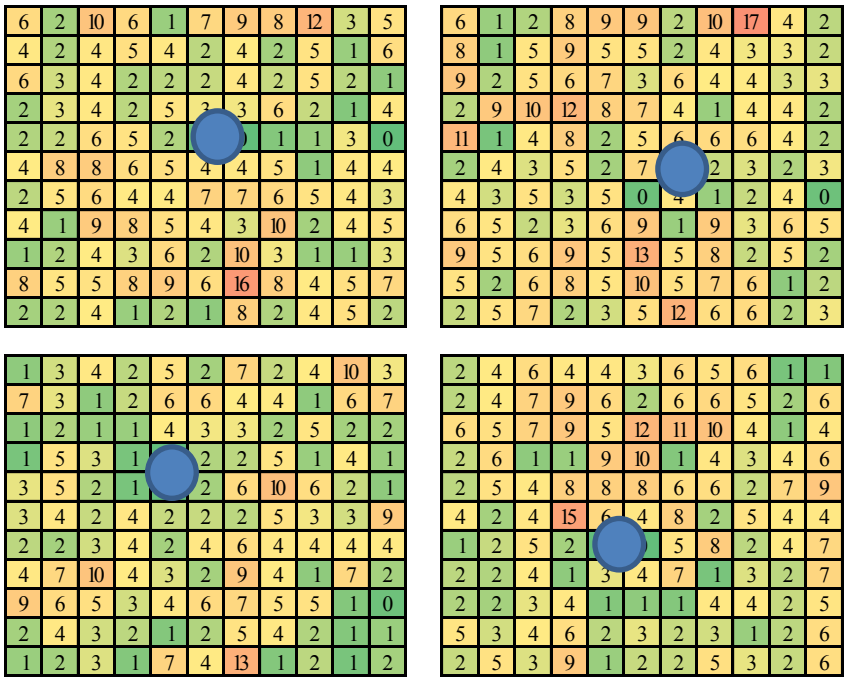

Figure 4-20 Damage mapping of YY-plane of biaxial specimen.

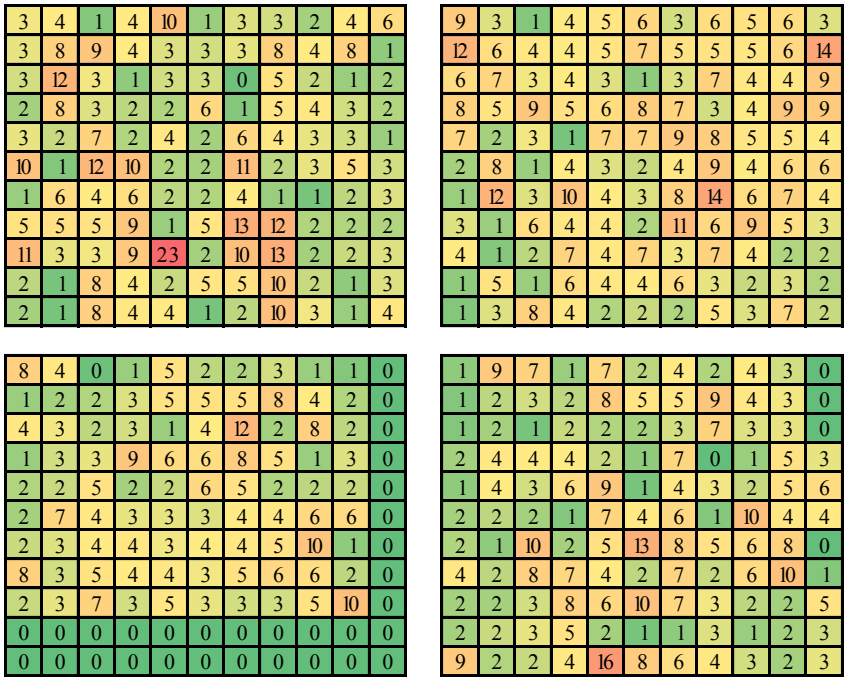

Figure 4-21 Damage mapping of ZZ-plane of biaxial specimen.

Chapter 5 Conclusions

The aim of this study was to investigate the influence of two types of restraint, namely uniaxial and biaxial and no-stress state in ASR-affected concrete pavement. The development of axial expansion and volumetric expansion due to ASR was carefully documented for 4.5 months and analyzed. The following conclusions can be pointed out:

1. The axial expansion measured in the unrestraint cube specimens were greater than those measured in uniaxial and biaxial cube specimens. For uniaxial and biaxial stress state, all three mutual perpendicular planes were expanding but expansion in unrestraint direction was considerably high. Expansion was directly proportional to the amount of stress applied.
2. Expansion reduced in the direction of stress applied in both the stress state and transferred to the unrestraint direction. For unrestraint specimens, three different planes expanded uniformly with small variation while for uniaxial and biaxial stress state the unrestraint volumetric expansion accounted for 78% and 52% of total expansion respectively.
3. DRI test showed that the ASR-induced damage varies with different stress state. The DRI values for unrestraint cube specimens were considerably higher than the biaxial and uniaxial stress state concrete specimens. The confinement stresses were unable to suppress reaction but were successful to reduce the degree of damage. Damages such as open cracks in aggregate (OCCA), cracks in cement paste (CCP) and aggregate debonded (CAD) were largely reduced by confinement stress in concrete cube specimens.

4. The damage due to ASR were largely located in the mid area of the specimens rather than boundary area as seen in the damage map.

Finally, this research points out the complexity of anisotropic ASR expansion in different stress state, cracking and internal damage in concrete pavement. The result of 6 months of data has been presented in this paper. Further monitoring of the concrete cube specimens will be required to determine the ultimate expansion due to ASR under the accelerated conditions. DRI test at different expansion should be carried out which will shed more information in degree of damage due to different stress state. Similar an expanded study with different type of reactive aggregate with different mix design and sizes of specimen will be beneficial for better understanding of the ASR in restrained conditions

References

Ahmed, Tarig, et al. "The Effect of Alkali Reactivity on the Mechanical Properties of Concrete." *Construction and Building Materials*, vol. 17, no. 2, 2003, pp. 123–44.

ASTM C39. "Standard Test Method for Compressive Strength of Cylindrical Concrete Specimens." *ASTM International*, 2001.

ASTM C469. "Standard Test Method for Static Modulus of Elasticity and Poisson's Ratio of Concrete in Compression." *ASTM International*, 2014.

ASTM C1260. "Standard Test Method for Potential Alkali Reactivity of Aggregates (Mortar-Bar Method)." *ASTM International, West Conshohocken, United States*, 2001, p. 5.

ASTM C1293. "Standard Test Method for Determination of Length Change of Concrete Due to Alkali–Silica Reaction." *West Conshohocken, PA: ASTM International*, vol. 7, 2008.

Berra, Mario, et al. "Influence of Stress Restraint on the Expansive Behaviour of Concrete Affected by Alkali-Silica Reaction." *Cement and Concrete Research*, vol. 40, no. 9, 2010, pp. 1403–09.

Dunbar, P. A., and P. E. Grattan-Bellew. *Results of Damage Rating Evaluation of Condition of Concrete from a Number of Structures Affected by AAR*. 1995.

Fournier, B. "Report on the Diagnosis, Prognosis, and Mitigation of Alkali-Silica Reaction in Transportation Structures." *FHWA*, 2010.

Fujii, Masahiro, et al. "The Static and Dynamic Behaviour of Reinforced Concrete Beams with Cracking Due to Alkali-Silica Reaction--Proceedings of the 7th International

Conference on Concrete Alkali-Aggregate Reactions, Ottawa, Canada, 1986." *Publication of: Noyes Publications*, 1987.

Funahashi, Miki. "Predicting Corrosion-Free Service Life of a Concrete Structure." *ACI Materials Journal*, 1990.

Gautam, Bishnu Prasad. *Multiaxially Loaded Concrete Undergoing Alkali-Silica Reaction (ASR)*. University of Toronto (Canada), 2016.

Giaccio, G., et al. "Mechanical Behavior of Concretes Damaged by Alkali-Silica Reaction." *Cement and Concrete Research*, vol. 38, no. 7, 2008, pp. 993–1004.

Giebson, Colin, et al. "Influence of Acetate and Formate-Based Deicers on ASR in Airfield Concrete Pavements." *Cement and Concrete Research*, vol. 40, no. 4, 2010, pp. 537–45.

Grattan-Bellew, P. E., and A. Danay. "Comparison of Laboratory and Field Evaluation of AAR in Large Dams." *Proceedings of the International Conference on Concrete Alkali–Aggregate Reactions in Hydroelectric Plants and Dams, Fredericton, NB*, vol. 28, 1992.

Grattan-Bellew, P. E., and L. D. Mitchell. "Quantitative Petrographic Analysis of Concrete-the Damage Rating Index (DRI) Method, a Review." *Proc. Marc-André Bérubé Symposium on AAR in Concrete, CANMET/ACI Advances in Concrete Technology Seminar, Montréal, Canada*, 2006, pp. 321–34.

Justice, J. M., et al. "Comparison of Two Metakaolins and a Silica Fume Used as Supplementary Cementitious Materials." *SP-228, ACI, Farmington Hills, Mich*, 2005, pp. 213–36.

Kagimoto, Hiroyuki, et al. “ASR Expansion, Expansive Pressure and Cracking in Concrete Prisms under Various Degrees of Restraint.” *Cement and Concrete Research*, vol. 59, 2014, pp. 1–15.

Latifee, Enamur R. “State-of-the-Art Report on Alkali Silica Reactivity Mitigation Effectiveness Using Different Types of Fly Ashes.” *Journal of Materials*, 2016, doi:10.1155/2016/7871206.

Le Roux, A., et al. “Evolution Under Stress of a Concrete Affected by AAR-Application to the Feasilbility of Strengthening a Bridge by Prestressing.” *The Ninth International Conference on Alkali-Aggregate Reaction in Concrete.*, vol. 2, 1992.

Lindgård, Jan, et al. “Alkali–Silica Reaction (ASR)—Performance Testing: Influence of Specimen Pre-Treatment, Exposure Conditions and Prism Size on Alkali Leaching and Prism Expansion.” *Cement and Concrete Research*, vol. 53, 2013, pp. 68–90.

Marzouk, H., and S. Langdon. “The Effect of Alkali-Aggregate Reactivity on the Mechanical Properties of High and Normal Strength Concrete.” *Cement and Concrete Composites*, vol. 25, no. 4–5, 2003, pp. 549–56.

Moranville-Regourd, M. “Modelling of Expansion Induced by ASR — New Approaches.” *Cement and Concrete Composites*, vol. 19, no. 5, Jan. 1997, pp. 415–25.

Morenon, Pierre, et al. “Impact of Stresses and Restraints on ASR Expansion.” *Construction and Building Materials*, vol. 140, 2017, pp. 58–74.

Multon, Stéphane, et al. “Effects of Aggregate Size and Alkali Content on ASR Expansion.” *Cement and Concrete Research*, vol. 40, no. 4, Apr. 2010, pp. 508–16.

Multon, Stéphane, and François Toutlemonde. "Effect of Applied Stresses on Alkali–Silica Reaction-Induced Expansions." *Cement and Concrete Research*, vol. 36, no. 5, 2006, pp. 912–20.

Phillips, William J. *Alkali Silica Reaction Mitigation Using High Volume Class c Fly Ash*. University of Arkansas, 2015.

Prezzi, Monica, et al. "The Alkali–Silica Reaction: Part I. Use of the Double-Layer Theory to Explain the Behavior of Reaction-Product Gels." *ACI Materials Journal*, vol. 94, no. 1, 1997, pp. 10–17.

Rivard, Patrice, et al. "The Damage Rating Index Method for ASR Affected Concrete—a Critical Review of Petrographic Features of Deterioration and Evaluation Criteria." *Cement, Concrete and Aggregates*, vol. 24, no. 2, 2002, pp. 1–11.

Rivard, Patrice, and François Saint-Pierre. "Assessing Alkali-Silica Reaction Damage to Concrete with Non-Destructive Methods: From the Lab to the Field." *Construction and Building Materials*, vol. 23, no. 2, 2009, pp. 902–09.

Sanchez, L. F. M., B. Fournier, M. Jolin, and Josée Duchesne. "Reliable Quantification of AAR Damage through Assessment of the Damage Rating Index (DRI)." *Cement and Concrete Research*, vol. 67, 2015, pp. 74–92.

Sanchez, L. F. M., B. Fournier, M. Jolin, M. A. B. Bedoya, et al. "Use of Damage Rating Index to Quantify Alkali-Silica Reaction Damage in Concrete: Fine versus Coarse Aggregate." *ACI Materials Journal*, vol. 113, no. 4, 2016.

Sanchez, Leandro. *Contribution to the Assessment of Damage in Aging Concrete Infrastructures Affected by Alkali-Aggregate Reaction*. Citeseer, 2014.

Sargolzahi, Maryam, et al. “Effectiveness of Nondestructive Testing for the Evaluation of Alkali–Silica Reaction in Concrete.” *Construction and Building Materials*, vol. 24, no. 8, 2010, pp. 1398–403.

Sellier, A., et al. “Modeling the Alkali-Aggregate Reaction with Descriptions of the Local Destructive Phenomena Involved.” *Materials and Structures*, vol. 28, no. 181, 1995, pp. 373–83.

Shrimer, Fred, et al. “Application and Use of Damage Rating Index in Assessment of AAR-Affected Concrete–Selected Case Studies.” *Proceedings of the 11th International Conference on AAR in Concrete, Quebec City, Canada*, 2000, pp. 899–908.

Smaoui, Nizar, et al. “Mechanical Properties of ASR-Affected Concrete Containing Fine or Coarse Reactive Aggregates.” *Journal of ASTM International*, vol. 3, no. 3, 2005, pp. 1–16.

Stanton, Thomas E. *Expansion of Concrete Through Reaction Between Cement and Aggregate*. 2008.

Stark, David. “The Moisture Condition of Field Concrete Exhibiting Alkali-Silica Reactivity.” *Special Publication*, vol. 126, 1991, pp. 973–88.

Swamy, R. N., and M. M. Al-Asali. “Engineering Properties of Concrete Affected by Alkali-Silica Reaction.” *ACI Materials Journal*, vol. 85, no. 5, 1988, pp. 367–74.

Swamy, R. Narayan. *The Alkali-Silica Reaction in Concrete*. CRC Press, 2002.

Takahashi, Y., et al. “Uniaxial Restraint Tests Under High-Stress Conditions and a Chemo-Hygral Model for Asr Expansion.” *Concreep 10*, 2015, pp. 1061–65.

The Institution of Structural Engineers. *Structural Effects of Alkali-Silica Reaction: Technical Guidance on the Appraisal of Existing Structures*. Institution of structural engineers, 1992.

Thomas, M. D. A., et al. *Alkali-Silica Reactivity Field Identification Handbook*. 2011.

Thomas, Michael, et al. "Test Methods for Evaluating Preventive Measures for Controlling Expansion Due to Alkali–Silica Reaction in Concrete." *Cement and Concrete Research*, vol. 36, no. 10, Oct. 2006, pp. 1842–56.

Thomas, Michael DA, et al. *Methods for Evaluating and Treating ASR-Affected Structures: Results of Field Application and Demonstration Projects–Volume II: Details of Field Applications and Analysis*. 2013.

Villeneuve, V., et al. "Determination of the Damage in Concrete Affected by ASR–the Damage Rating Index (DRI)." *14th International Conference on Alkali-Aggregate Reaction (ICAAR). Austin, Texas (USA)*, 2012.

Appendices

Appendix A High-Strength Bolt and Bearing Plate Design

High-Strength Bolt Design

Total stress applied (P) = 3.5 MPa ≈ 507.63 psi

Choose Class 10M threaded bolt

Yield Strength (σ) = 900 MPa ≈ 130534 psi

Tensile Strength = 1000 MPa ≈ 145038 psi

Area of cube = 100 in^2

Stress per bolt (P_b) = $\frac{PA}{4} = \frac{507.63 \times 100}{4} = 12690.75$ lb.

$$\text{Area } (A) = \frac{P_b}{\sigma} = \frac{12690.75}{130534} = 0.097 \text{ in}^2$$

$$\frac{\pi d^2}{4} = 0.097 \text{ in}^2$$

$$\therefore d = 0.35 \text{ in.}$$

Therefore, use 0.5 in. diameter bolt.

Bearing Plate Design

Area of cube = 100 in^2

Stress applied (σ) = 3.5 MPa ≈ 507.63 psi

Use ASTM 108 1018 alloy steel base plate

Yield Strength = 55000 psi

Tensile Strength = 65000 psi

Total Stress (P_u) = σA = 507.63 x 100 = 50763 lb.

Stress per plate (P_b) = $\frac{P_c}{4} = \frac{50763}{4} = 12690.75$ lb.

Area of Base Plate = $\frac{P_b}{0.85f_c^{'}} = \frac{12690.75}{0.85\times4500} = 3.31\ in^2$

$\therefore$ N=B=1.7 in.

Thickness of base plate (t) = $\left(\frac{3\text{-}3/4}{2}\right)\sqrt{\frac{2P_b}{NBF_y}} = 1.125\sqrt{\frac{2\times12690.75}{3\times3\times55000}} = 0.25$ in.

Therefore, use 1/2 x 3 x 3 in. base plate.

Appendix B Accelerated Mortar Bar Test of Jobe Sand

The sand was tested to determine the potential reactivity using the accelerated mortar bar test, based on ASTM C1260. The casting and storage method is shown in the Figure B-1. The axial expansion data for Jobe sand and non-reactive are tabulated in the Table B-1 and Table B-2 respectively.

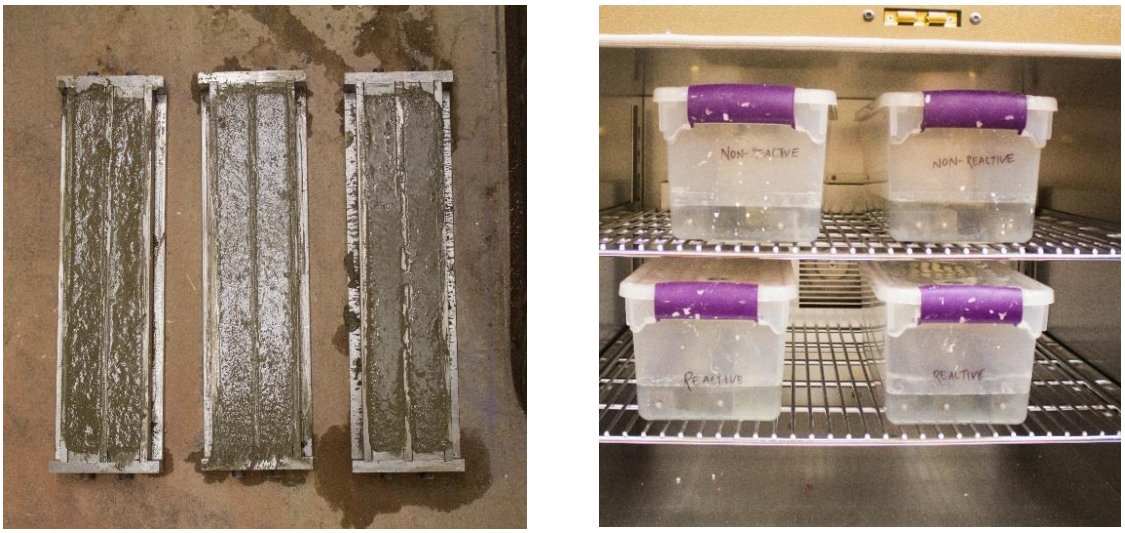

Figure B-1 (a) Casting of 6 test specimens for AMBT test. (b) Concrete prisms stored at 80 ºC in 1N NaOH solution.

Table B-1 Axial expansion (%) of mortar bar using Jobe Sand.

S.N	Expansion (%)				
	3/11/2018	**3/15/2018**	**3/22/2018**	**3/29/2018**	**4/5/2018**
1	0.2735	0.3908	0.385	0.475	0.5395
2	0.27	0.3685	0.356	0.443	0.5095
3	0.221	0.336	0.2925	0.3985	0.4635
4	0.2355	0.3485	0.3245	0.41565	0.4725
5	0.2485	0.369	0.347	0.4425	0.4945

Table B-2 Axial expansion (%) of mortar bar using Non-reactive sand.

S.N	Expansion (%)				
	3/11/2018	**3/15/2018**	**3/22/2018**	**3/29/2018**	**4/5/2018**
1	0.044	0.105	0.101	0.885	0.2315
2	0.032	0.093	0.0885	0.1795	0.2165
3	0.051	0.112	0.111	0.19	0.223
4	0.0275	0.0695	0.075	0.1795	0.223
5	0.031	0.071	0.074	0.1525	0.2045

Appendix C Concrete Prism Test of Jobe Sand

Another aggregate reactivity test is the concrete prism test using ASTM C1293 method. It is a yearlong test. But only 6 months of data is presented in here in this study. The storage method and expansion measurement is shown in the Figure C-1 below. The expansion data are also shown in the Table C-1 below.

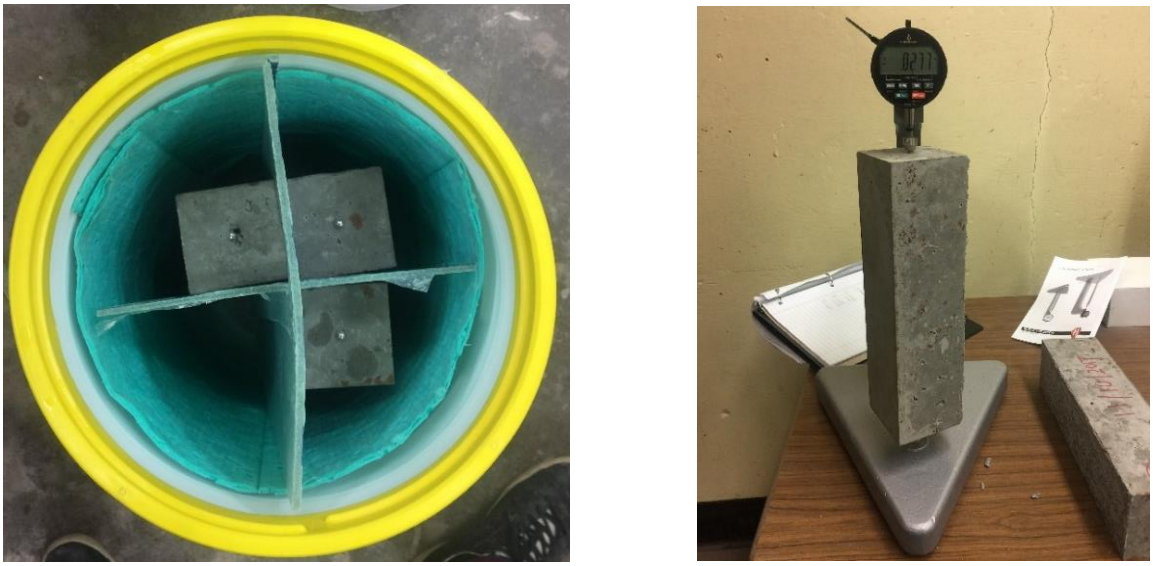

Figure C-2 (a) Top view of test prisms being stored over water inside the bucket. (b) Measuring a concrete prism for length change using a micrometer.

Table C-3 Axial expansion (%) of concrete prism specimen using Jobe Sand.

Batch	S.N	Expansion (%)				
		11/16/2017	12/7/2017	1/16/2018	2/7/2018	5/8/2018
1st	1	0.017	0.1505	0.2685	0.3345	0.3945
	2	0.0255	0.114	0.2745	0.292	0.3645
	3	0.2475	0.2578	0.27055	0.27335	0.2819
2nd	1	0.0145	0.124	0.246	0.3065	0.392
	2	0.013	0.1565	0.2665	0.2795	0.354
	3	0.0175	0.1175	0.2725	0.2955	0.3585

Appendix D Compressive Strength and Modulus of Elasticity Test

The average modulus of elasticity and the compressive strength at the age of 28 day was 4486090 psi and 6012 psi respectively. The set up for the tests are show in the Figure D-1 and Figure D-2.

Figure D-3 Failure of concrete cylinder under the Compression Strength Test.

Figure D-4 A concrete cylinder undergoing EOM test.

Appendix E Strain Measurement of Concrete Cube Specimen

The expansion data for unrestrained, uniaxial and biaxial concrete cubes are shown in the Table E-1, Table E-2 and Table E-3 respectively.

Table E-4 Expansion data of unrestrained concrete cubes.

S.N	Date	Average expansion value of each axis			
		Days	X	Y	Z
1	1/16/2018	0	0	0.0000	0
2	1/30/2018	14	-0.0106	-0.0097	-0.0040
3	2/6/2018	21	0.0021	0.0018	0.0046
4	2/13/2018	28	-0.0018	-0.0019	0.0000
5	2/23/2018	38	-0.0038	-0.0094	-0.0043
6	3/4/2018	47	0.0239	0.0101	0.0263
7	3/11/2018	54	0.0389	0.0236	0.0397
8	3/18/2018	61	0.0696	0.0625	0.0765
9	3/25/2018	68	0.0861	0.0771	0.0900
10	4/1/2018	75	0.0947	0.0931	0.1021
11	4/8/2018	82	0.1172	0.1174	0.1289
12	4/15/2018	89	0.1514	0.1586	0.1621
13	4/22/2018	96	0.1751	0.1915	0.1964
14	5/13/2018	117	0.2169	0.2281	0.2371
15	5/31/2018	135	0.2373	0.2471	0.2552

Table E-5 Expansion data of uniaxial concrete cubes.

S.N	Date	Average expansion value of each axis			
		Days	X	Y	Z
1	1/16/2018	0	0	0.0000	0
2	1/30/2018	14	-0.0076	0.0150	0.0007
3	2/6/2018	21	-0.0075	0.0097	0.0053
4	2/13/2018	28	-0.0063	0.0067	0.0026
5	2/23/2018	38	-0.0076	0.0037	0.0035
6	3/4/2018	47	0.0133	0.0251	0.0271
7	3/11/2018	54	-0.0079	0.0125	0.0132
8	3/18/2018	61	0.0294	0.0542	0.0561
9	3/25/2018	68	0.0443	0.0843	0.0813
10	4/1/2018	75	0.0403	0.0868	0.0908
11	4/8/2018	82	0.0372	0.0879	0.0906
12	4/15/2018	89	0.0514	0.1189	0.1236
13	4/22/2018	96	0.0711	0.1493	0.1433
14	5/13/2018	117	0.0950	0.2021	0.1963
15	5/31/2018	135	0.1290	0.2415	0.2279

Table E-6 Expansion data of biaxial concrete cubes.

S.N	Date	Average expansion value of each axis			
		Days	X	Y	Z
1	1/16/2018	0	0	0.0000	0
2	1/30/2018	14	0.0031	0.0058	0.0047
3	2/6/2018	21	0.0054	0.0032	0.0050
4	2/13/2018	28	0.0074	0.0040	0.0058
5	2/23/2018	38	0.0050	0.0001	0.0039
6	3/4/2018	47	0.0558	0.0460	0.0331
7	3/11/2018	54	0.0382	0.0276	0.0095
8	3/18/2018	61	0.0674	0.0481	0.0244
9	3/25/2018	68	0.0675	0.0336	0.0156
10	4/1/2018	75	0.1054	0.0693	0.0490
11	4/8/2018	82	0.0874	0.0406	0.0219
12	4/15/2018	89	0.1275	0.0615	0.0364
13	4/22/2018	96	0.1418	0.0783	0.0542
14	5/13/2018	117	0.1704	0.0808	0.0602
15	5/31/2018	135	0.2365	0.1202	0.0933